Author Manuscript Published OnlineFirst on April 1, 2020; DOI: 10.1158/2159-8290.CD-19-1030
Author manuscripts have been peer reviewed and accepted for publication but have not yet been edited.

Infant high grade gliomas comprise multiple subgroups characterized by novel targetable gene fusions and favorable outcomes

Matthew Clarke[1], Alan Mackay[1*], Britta Ismer[2,3,4*], Jessica C Pickles[5], Ruth G Tatevossian[6], Scott Newman[7], Tejus A Bale[8], Iris Stoler[9], Elisa Izquierdo[1], Sara Temelso[1], Diana M Carvalho[1], Valeria Molinari[1], Anna Burford[1], Louise Howell[1], Alex Virasami[5], Amy R Fairchild[5], Aimee Avery[5], Jane Chalker[5], Mark Kristiansen[5], Kelly Haupfear[6], James D Dalton[6], Wilda Orisme[6], Ji Wen[6], Michael Hubank[10], Kathreena M Kurian[11], Catherine Rowe[11], Mellissa Maybury[12,13,14], Stephen Crosier[15], Jeffrey Knipstein[16], Ulrich Schüller[17,18], Uwe Kordes[18], David E Kram[19], Matija Snuderl[20], Leslie Bridges[21], Andrew J Martin[22], Lawrence J Doey[23], Safa Al-Sarraj[23], Christopher Chandler[24], Bassel Zebian[24], Claire Cairns[24], Rachael Natrajan[25], Jessica KR Boult[26], Simon P Robinson[26], Martin Sill[2], Ira J Dunkel[27], Stephen W Gilheeney[27], Marc K Rosenblum[8], Debbie Hughes[10], Paula Z Proszek[10], Tobey J Macdonald[28], Matthias Preusser[29], Christine Haberler[29,30], Irene Slavc[31], Roger Packer[32], Ho-keung Ng[33], Shani Caspi[34], Mara Popović[35], Barbara Faganel Kotnik[36], Matthew D Wood[37], Lissa Baird[38], Monika Ashok Davare[39], David A Solomon[40,41], Thale Kristin Olsen[42], Petter Brandal[43], Michael Farrell[44], Jane B Cryan[44], Michael Capra[45], Michael Karremann[46], Jens Schittenhelm[47], Martin U Schuhmann[48], Martin Ebinger[49], Winand NM Dinjens[50], Kornelius Kerl[51], Simone Hettmer[52], Torsten Pietsch[53], Felipe Andreiuolo[53], Pablo Hernáiz Driever[54], Andrey Korshunov[55], Lotte Hiddingh[2], Barbara C Worst[2,4,56], Dominik Sturm[2,4,56], Marc Zuckermann[2,4], Olaf Witt[2,4,56], Tabitha Bloom[57], Clare Mitchell[57], Evelina Miele[58], Giovanna Stefania Colafati[59], Francesca Diomedi-Camassei[60], Simon Bailey[15], Andrew S Moore[12,13,14], Timothy EG Hassall[13,61,62], Stephen P Lowis[11], Maria Tsoli[63,64], Mark J Cowley[63.64], David S Ziegler[63,64], Matthias A Karajannis[27], Kristian Aquilina[65], Darren R Hargrave[66], Fernando Carceller[67,68], Lynley V Marshall[67,68], Andreas von Deimling[55,69], Christof M Kramm[70], Stefan M Pfister[2,4,56], Felix Sahm[54,69], Suzanne J Baker[71], Angela Mastronuzzi[72], Andrea Carai[73], Maria Vinci[58], David Capper[9,74], Sergey*

Popov[1,75], David W Ellison[6#], Thomas S Jacques[5#], David TW Jones,[2,4#], and Chris Jones[1#]

[1]Division of Molecular Pathology, Institute of Cancer Research, London, UK; [2]German Cancer Research Center (DKFZ); [3]Faculty of Biosciences, Heidelberg University, Heidelberg, Germany; [4]Hopp Children's Cancer Center Heidelberg (KiTZ), Heidelberg, Germany; [5]UCL Great Ormond Street Institute of Child Health, London, UK; [6]Department of Neuropathology, St Jude Children's Research Hospital, Memphis TN, USA; [7]Department of Computational Biology, St Jude Children's Research Hospital, Memphis TN, USA; [8]Department of Neuropathology, Memorial Sloan-Kettering Cancer Center, New York NY, USA; [9]Charité Universitätsmedizin Berlin, corporate member of Freie Universität Berlin, Humboldt-Universität zu Berlin, and Berlin Institute of Health, Department of Neuropathology, Berlin, Germany; [10]Molecular Diagnostics, Royal Marsden Hospital NHS Trust, Sutton, UK; [11]Brain Tumour Research Centre, University of Bristol, Bristol, UK; [12]The University of Queensland Diamantina Institute, The University of Queensland, Woolloongabba, Australia; [13]Oncology Service, Queensland Children's Hospital, Brisbane, Australia; [14]Child Health Research Centre, The University of Queensland, South Brisbane, Australia; [15]Newcastle Hospitals NHS Foundation Trust, Newcastle, UK; [16]Division of Pediatric Hematology/Oncology/BMT, Medical College of Wisconsin, Milwaukee WI, USA; [17]Department of Neuropathology, University Hospital Hamburg-Eppendorf, and Research Institute Children's Cancer Center, Hamburg, Germany; [18]Pediatric Hematology and Oncology, University Hospital Hamburg-Eppendorf, Hamburg, Germany; [19]Section of Pediatric Hematology-Oncology, Wake Forest School of Medicine, Winston-Salem NC, USA; [20]Department of Neuropathology, NYU Langone Health, New York NY, USA; [21]Department of Neuropathology, St George's Hospital NHS Trust, London, UK; [22]Department of Neurosurgery, St George's Hospital NHS Trust, London, UK; [23]Department of Clinical Neuropathology, Kings College Hospital NHS Trust, London, UK; [24]Department of Neurosurgery, Kings College Hospital NHS Trust, London, UK; [25]The Breast Cancer Now Toby Robins Research Centre, The Institute of Cancer Research, London, UK; [26]Division of Radiotherapy and Imaging, The Institute of Cancer Research, London, UK; [27]Department of Pediatrics, Memorial Sloan-Kettering Cancer Center, New York NY, USA; [28]Aflac Cancer and Blood Disorders Center, Department of Pediatrics, Emory University School of Medicine, Atlanta GA, USA; [29]Comprehensive Cancer Center, Medical University of Vienna, Vienna, Austria; [30]Institute of Neurology, Medical University of Vienna, Vienna, Austria; [31]Department of Pediatrics and Adolescent Medicine, Medical University of Vienna, Vienna, Austria; [32]Center for Neuroscience and Behavioural Medicine, Children's National Medical Center, Washington DC, USA; [33]Department of Anatomical and Cellular Pathology, The Chinese University of Hong Kong,

China; [34]Cancer Research Center, Sheba Medical Center, Tel Aviv, Israel; [35]Faculty of Medicine, University of Ljubljana, Ljubljana, Slovenia; [36]Department of Hematology and Oncology, University Children's Hospital, Ljubljana, Slovenia; [37]Department of Pathology, Oregon Health & Science University, Portland OR, USA; [38]Department of Neurosurgery, Oregon Health & Science University, Portland OR, USA; [39]Department of Pediatrics, Oregon Health & Science University, Portland OR, USA; [40]Department of Pathology, University of California, San Francisco, CA, United States; [41]Clinical Cancer Genomics Laboratory, University of California, San Francisco, CA, United States; [42]Department of Women's and Children's Health, Karolinska Institute, Stockholm, Sweden; [43]Department of Oncology, Oslo University Hospital, Oslo, Norway; [44]Department of Histopathology, Beaumont Hospital, Dublin, Ireland; [45]Paediatric Oncology, Our Lady's Children's Hospital, Dublin, Ireland; [46]Department of Pediatrics, University Medical Center Mannheim, Medical Faculty Mannheim, Heidelberg University, Mannheim, Germany; [47]Institute of Pathology and Neuropathology, University Hospital Tübingen, Germany; [48]Department of Neurosurgery, University Hospital Tübingen, Germany; [49]Department of Pediatric Hematology and Oncology, University Hospital Tübingen, Germany; [50]Department of Pathology, Erasmus Medical Center, Rotterdam, Netherlands; [51]Department of Pediatric Hematology and Oncology, University Hospital Muenster, Germany; [52]Department of Pediatric Hematology and Oncology, University Hospital Freiburg, Germany; [53]Institute of Neuropathology, DGNN Brain Tumor Reference Center, University of Bonn Medical Center, Bonn, Germany; [54]Department of Paediatric Haematology/Oncology Charité Universitätsmedizin, Berlin, Germany; [55]Department of Neuropathology, University Hospital Heidelberg, Germany; [56]Department of Pediatric Oncology, Hematology, Immunology and Pulmonology, Heidelberg University Hospital, 69120 Heidelberg, Germany; [57]BRAIN UK, University of Southampton, Southampton, UK; [58]Department of Onco-haematology, Cell and Gene Therapy, Bambino Gesù Children's Hospital-IRCCS, Rome, Italy; [59]Oncological Neuroradiology Unit, Department of Diagnostic Imaging, Bambino Gesù Children's Hospital-IRCCS, Rome, Italy; [60]Department of Laboratories - Pathology Unit, Bambino Gesù Children's Hospital-IRCCS, Rome, Italy; [61]Institute for Molecular Bioscience, The University of Queensland, St Lucia, Australia; [62]School of Biomedical Sciences, Faculty of Health, Queensland University of Technology, Brisbane, Australia; [63]Children's Cancer Institute, University of New South Wales, Sydney, Australia; [64]Kids Cancer Centre, Sydney Children's Hospital, Randwick, Australia; [65]Department of Neurosurgery, Great Ormond Street Hospital NHS Foundation Trust, London, UK; [66]Department of Paediatric Oncology, Great Ormond Street Hospital NHS Foundation Trust, London, UK; [67]Division of Clinical Studies, The Institute of Cancer Research, London, UK; [68]Children & Young People's Unit, Royal Marsden Hospital NHS Trust, Sutton, UK; [69]Clinical Cooperation Unit Neuropathology, German Cancer Consortium (DKTK), German Cancer Research Center (DKFZ), Heidelberg, Germany; [70]Division of Pediatric Hematology and

Oncology, University Medical Centre Göttingen, Germany; [71]Department of Neurobiology, St Jude Children's Research Hospital, Memphis TN, USA; [72]Neuro-oncology Unit, Department of Onco-haematology, Cell and Gene Therapy, Bambino Gesù Children's Hospital-IRCCS, Rome, Italy; [73]Oncological Neurosurgery Unit, Department of Neuroscience and Neurorehabilitation, Bambino Gesù Children's Hospital-IRCCS, Rome, Italy; [74]German Cancer Consortium (DKTK), Partner Site Berlin, German Cancer Research Center (DKFZ), Heidelberg, Germany; [75]Department of Pathology, University of Wales Hospital NHS Trust, Cardiff, UK

* *These authors contributed equally*

[#]*Correspondence to:*

Chris Jones,

Division of Molecular Pathology, The Institute of Cancer Research, 15 Cotswold Road, Sutton, Surrey, SM2 5NG, UK, chris.jones@icr.ac.uk, +44 (0)20 8722 4416

David TW Jones,

Hopp Children's Cancer Center Heidelberg (KiTZ) and German Cancer Research Center (DKFZ), Im Neuenheimer Feld 280, 69120 Heidelberg, Germany, david.jones@kitz-heidelberg.de, +49 6221 42-4675

Thomas S Jacques,

UCL GOS Institute of Child Health, 30 Guilford Street, London WC1N 1EH, UK, t.jacques@ucl.ac.uk, +44 (0)20 7762 6108

David W Ellison

Department of Pathology, St Jude Children's Research Hospital, 262 Danny Thomas Place, Memphis, TN 38105-3100, USA, david.ellison@stjude.org, +1 901 595-3533

Conflict of interest statement

The authors declare no conflict of interest

Keywords: infant, glioma, methylation, sequencing, NTRK, ALK, ROS1

Running title: Classification of infant glioma

Abstract

Infant high grade gliomas appear clinically distinct from their counterparts in older children, indicating that histopathologic grading may not accurately reflect the biology of these tumors. We have collected 241 cases under 4 years of age, and carried out histological review, methylation profiling, custom panel and genome/exome sequencing. After excluding tumors representing other established entities or subgroups, we identified 130 cases to be part of an 'intrinsic' spectrum of disease specific to the infant population. These included those with targetable MAP-kinase alterations, and a large proportion of remaining cases harboring gene fusions targeting *ALK* (n=31), *NTRK1/2/3* (n=21), *ROS1* (n=9) and *MET* (n=4) as their driving alterations, with evidence of efficacy of targeted agents in the clinic. These data strongly supports the concept that infant gliomas require a change in diagnostic practice and management.

Statement of Significance

Infant high grade gliomas in the cerebral hemispheres comprise novel subgroups, with a prevalence of *ALK*, *NTRK1-3*, *ROS1* and *MET* gene fusions. Kinase fusion-positive tumors have better outcome and respond to targeted therapy clinically. Other subgroups have poor outcome, with fusion-negative cases possibly representing an epigenetically-driven pluripotent stem cell phenotype.

Introduction

The prognosis of paediatric high grade gliomas (HGG) remains dismal, with a 5-year survival rate of only ~20% for children aged 0-14 years (1). They are strongly associated with unique location-dependent mutations in histone H3 variants H3.3 (*H3F3A*) and H3.1 (*HIST1H3B/C*) including two recurrent amino acid substitutions (K27M and G34R/V) (2,3) which together account for nearly half of all paediatric HGG and identify robust biological subgroups (4,5). Histone wild-type cases are comprised of a highly diverse set of tumors, ranging from those with some of the highest somatic mutational burdens in human cancer (patients with biallelic mismatch repair deficiency syndrome) (6,7) to others seemingly driven by single genetic events, often gene fusions (8). The latter are particularly found in cases originally diagnosed as high grade glioma at an infant age (9).

The definition of an infant used in paediatric neuro-oncology varies, but typically refers to children under 3-5 years (10); congenital cases are generally defined as being present at birth (11). The most frequent types of infant brain tumor are medulloblastoma, ependymomas and low grade gliomas (LGG) (12). The latter include the relatively common pilocytic astrocytomas, but also other rarer entities such as desmoplastic infantile ganglioglioma/astrocytoma (DIGG/DIA) (13). Tumors reported as HGG appear to be associated with significant differences in clinical outcome, with infant HGG (even with incomplete resection and without irradiation) showing a significantly improved survival compared to those in older children (8,14-17), which may indicate the presence of a distinct, overlapping group of tumors where histopathologic grading may not be representative of clinical behavior.

Treatment outcomes also reflect these differences; the Baby POG I study found four children under 3 years of age who were diagnosed with a malignant glioma and underwent 24 months of chemotherapy without radiation treatment, and did not

develop recurrent disease (10). A 5-year overall survival rate of 59% was reported in infants with HGG after prolonged chemotherapy treatment alone, and in another study, 16 patients diagnosed with HGG and treated with focal radiation therapy showed a 5-year overall survival rate of 66% (11). Five reported cases of congenital glioblastomas who survived surgery (with only one patient receiving a gross total resection) all showed a better outcome than expected (18), whilst two infant cases who both underwent subtotal resection of their tumors and did not receive any adjuvant therapy post-operatively saw regression of the residual tumors (19). The improved outcome both with chemotherapy and with surgery alone is particularly significant in this age group when considering the risk of declining cognition (13) and the development of leukoencephalopathy post radiation treatment (11).

Previous studies have hinted at different histological features within infant high grade gliomas. High densities of ‘minigemistocytic shaped’ cells with abundant mitoses and absent necrosis were described (20), with others showing moderately hypercellular, mitotic and necrotic tumors with cellular monotony and a lack of significant pleomorphism, and some showing a more spindled appearance (18,19).

Current molecular data is limited, but epidermal growth factor receptor (*EGFR*) and platelet-derived growth factor receptor A (*PDGFRA*) expression is reported as uniformly low in congenital glioblastomas (GBM), with a low level or absence of copy number alterations in these genes (18,21). *TP53* and *PTEN* mutations, *CDKN2A/B* deletions, and other copy number alterations often seen in older children are also not typically found in infant HGG (22). Occasional *BRAF* V600E mutations are found, particularly in DIGG/DIA (23), while histone and *IDH1* mutations are rare. Methylation profiling indicates that the infant group may display a more LGG-like methylation pattern, with a 2-year survival of 74% (8). The most common somatic alterations seen in infants appear to be gene fusion events, particularly *NTRK1/2/3.* Although

not specific to brain tumors (24), these were found to span both LGG and HGG in large-scale studies in children, with novel *QKI-NTRK2* and *NACC2-NTRK2* fusions found in pilocytic astrocytomas (25,26), and *AGBL4:NTRK2*, *TPM3:NTRK1*, and *ETV6:NTRK3* fusions found in HGG patients aged less than 3 years (9). More recently, several case reports have identified additional receptor tyrosine kinase (RTK) gene fusions in infant glioma of differing histologies (17,27-35).

In the present study, we collected the largest series of infant gliomas (exclusive of pilocytic astrocytomas) assembled to date and present a classification system based on integrated methylation profiling, fusion gene analysis, mutation detection, and histological review, with preclinical and clinical evidence of effective targeting of the driving alterations in these unique entities.

Results

Refinement of an intrinsic set of infant hemispheric gliomas

We collected a unique series of 241 gliomas, from patients under the age of four years at diagnosis from multiple centres around the world, with a view to exclude *a priori* pilocytic astrocytomas and other well characterised, low grade lesions with clear molecular markers (Figure 1A). To ensure this, we searched for pathognomonic structural variants using a variety of sequencing platforms including whole genome, exome, RNAseq and a novel custom capture panel (Figure 1B). We identified 28 cases to be excluded, mostly due to presence of *KIAA1549:BRAF* fusions (n=22), the vast majority of which were collected as an otherwise unspecified cerebellar astrocytoma (Supplementary Table S1). We also identified three cases of *FGFR1* tandem duplication (including glioneuronal tumors), two *MYB/MYBL1* fusions, and a case with *MN1:BEND2* (representing the novel entity of HGNET-MN1 (36)). Of the remaining 213 cases, a further 13 were excluded based on clear Heidelberg classifier matches to other non-glioma CNS tumors from methylation array profiling data (Figure 1C). These included two ependymomas, two HGNET-BCORs, an ETMR and others (Supplementary Figure S1). A further 9 cases failed array QC and were excluded from further analysis. Finally, our series of 191 cases were projected onto a reference set of gliomas comprising multiple entities. Sixty-one of these infant samples most readily clustered with a known high or low grade subtype, leaving us 130 infant gliomas for further analysis that we define as our ‘intrinsic set’ (Figure 1D), as they comprise a novel grouping of tumours with key clinical and molecular features in common, as we describe below.

The infant glioma cases excluded on the basis of methylation profiling (n=61) were found to have arisen in anatomical areas of the CNS appropriate for the relative subgroup assignment, such as diffuse midline glioma K27M mutant cases in the pons, pilocytic astrocytoma-like cases in the cerebellum, and PXA-like cases in the

cerebral hemispheres (Figure 1E), and were often accompanied by the expected genetic alteration. Interestingly, the remaining intrinsic set included the vast majority of those patients diagnosed under the age of 1 year (49/63, 78%; overall median of intrinsic set = 7.2 months). These cases scored most highly as two named subgroups in the current version (v11b4) of the methylation classifier – desmoplastic infantile ganglioglioma / astrocytoma (DIGG/DIA) and the poorly defined infant hemispheric glioma (IHG) (Supplementary Table S2). The vast majority of these cases were found in the cortex, DIGG/DIAs particularly in the frontal lobe. These cases were found to have a significantly improved outcome compared to cases classified as high grade gliomas (HGG), with a median overall survival similar to those considered as low grade gliomas (LGG) (Figure 1F), with the important caveat that detailed treatment information was not available across the cohort. The HGG subtype exclusions were predominantly >1 year old and showed a tendency towards a worse outcome than the other infant tumors (p=0.0567, log-rank test). This remaining intrinsic group of tumors formed a continuum which clustered clearly apart from other glioma subgroups in a tSNE projection based upon methylation array data from the glioma reference set (n=1652) (Figure 1G). Many of these cases did not unequivocally classify as either IHG or DIGG/DIA despite their tight clustering, suggesting that the reference classes for these tumors likely needs expanding and updating.

Infant hemispheric gliomas are defined by presence or absence of receptor tyrosine kinase fusions

Additional gene sequencing (panel, exome or genome) was available for 65 cases, including 41 of the intrinsic set, all of whom had fusion analysis by panel or RNAseq. Samples excluded as representing other glioma subtypes were found to harbor mutations consistent with such tumors, including *IDH1* R132H, *H3F3A* and *HIST1H3B* K27M, as well as common co-segregating variants in *TP53*, *NF1*, *PTEN*,

PIK3CA and *ACVR1*, deletions of *CDKN2A/B* and amplification of *PDGFRA* (Figure 2A). These were almost entirely absent from the intrinsic set. Instead, 25/41 cases (61%) harbored fusions in either *ALK* (n=10), *NTRK1/2/3 (n*=2, 2 and 8, respectively) *ROS1* (n=2) or *MET* (n=1), usually in the absence of other alterations (Figure 2B). The fusion-positive cases were mostly classified as IHGs (n=21) or low-scoring DIGG/DIAs (n=4). Although *ALK* fusions were restricted to the intrinsic set, we observed *NTRK* fusions in other glioma subtypes (especially *NTRK2*, n=3). We additionally observed an *FGFR1:TACC1* fusion in the *IDH1* / *TP53* case (Figure 2A). High-scoring DIGG/DIAs and 'DIGG/DIA-like' tumors were found with *BRAF* V600E (n=3) or *PIK3R1* mutations and isolated mutations in bromodomain-containing genes (*BRD8*, *BRD4*, *BRD2*) and others (Figure 2B). A single case harbored amplifications in both *MYC* and *MYCN*, in addition to *TP53* and *PIK3CA* mutations. Although a proportion (<25%) of tumors were found with whole-arm DNA copy number changes, the majority of intrinsic cases harbored few if any large-scale copy number alterations (Supplementary Figure S2A) (Supplementary Table S3).

There were no differences in the number of copy number changes between fusion-positive and fusion-negative cases (p=0.567, t-test) (Supplementary Figure S2B). Notably, the only significant focal differences were those marking common gene fusions at the *ALK* and *NTRK3* loci (Supplementary Figure S2C). A novel and refined copy number analysis from the methylation array data identified such breakpoints in either intra-chromosomal (short gains or losses) or inter-chromosomal (imbalances) RTK fusion events in 53/71 (75%) cases across the whole cohort (Figure 3A-C). Across the intrinsic set as a whole, 65/130 (50%) cases were found to harbor structural variants targeting *ALK*, *NTRK1/2/3*, *ROS1* or *MET* (46/80, 57.5% IHGs), compared with 18 of the other 111 cases in the original series (16%; p<0.0001, Fisher's exact test) (Supplementary Figure S3A-C) (Supplementary Table S4). Where possible, these were validated through a combination of genome, RNA and/or Sanger

sequencing, and were frequently accompanied by detectable focal DNA copy number breakpoints within the fusion partners, as exemplified for *ETV6:NTRK3* (Figure 3D) and the novel *ZC3H7A:ALK* fusions (Figure 3E). The most commonly targeted genes in the intrinsic set included *NTRK1/2/3*, predominantly *ETV6:NTRK3*, but also recurrent *EML4:NTRK3* and *TPM3:NTRK1* fusions (Figure 3F). *NTRK2* was found with numerous novel partners (e.g. *KCTD16:NTRK2* and *AGBL4:NTRK2*) but were largely seen in other glioma subtypes occuring in the appropriate anatomical locations (e.g. H3K27M in midline regions) (Supplementary Table S4), suggesting an important difference in *NTRK2* compared to *NTRK1/3* fusion-positive cases. *ALK* fusions were the most common (n=39), were largely restricted to the intrinsic set, and included both intra- and inter-chromosomal rearrangements (Figure 3G), including both previously reported (*PPP1CB:ALK*, *EML4:ALK*, *HIP1:ALK*, *PRKAR2A:ALK, SPTBN1:ALK*) and novel fusions (*MAD1L1:ALK*, *MAP2:ALK*, *MSI2:ALK*, *SPECC1L1:ALK*, *SYNDIG1L:ALK*, *ZC3H7A:ALK*, *CLIP2A:ALK*) (Supplementary Table S4). Within the intrinsic set, there was a trend towards the presence of any fusion conferring a longer overall survival compared to those without (p=0.0687, log-rank test) (Figure 3H).

With whole genome sequencing of fusion-negative cases failing to identify consistent genetic drivers of this subtype of the disease (Supplementary Figure S4), we turned to the methylation data in order to further explore the heterogeneity within infant HGG. Hierarchical clustering on the basis of differential probes associated with the most common genetic alterations found, resulting in the separation of distinct sets of IHG subgroups in addition to clear DIGG/DIA and ‘DIGG/DIA-like’ tumors (Supplementary Figure S5A). Despite the presence of recurrent *NTRK* fusions, these infant gliomas clustered apart from mesenchymal tumors harbouring *ETV6:NTRK3*, including infantile fibrosarcoma and congenital mesoblastic nephroma (37) (Supplementary Figure S5B). Running methylation-based gene ontology analysis on

the differentially methylated regions (Supplementary Table S5) highlighted little overlap between *ALK* fusion, *NTRK* fusion and fusion-negative cases (total 9.5%) (Supplementary Figure S5C). *ALK* fusion cases were significantly associated with dysregulation of genes associated with glutamate receptors, synapses, signal transduction and morphogenic stages of development (Figure 4A), whilst *NTRK* fusion cases were linked with genes controlling neuronal differentiation and the earliest stages of embryogenesis, as well as signalling via the JNK cascade (Figure 4B). By contrast, fusion-negative cases were predominantly associated with the response to multiple endogenous stimuli, particularly the TGFβ pathway, and the regulation of stem cell pluripotency and cell fate (Figure 4C). Although only exploratory due to the small sample sizes, and needing independent validation in an independent cohort, as exemplars of the differential epigenetic regulation of key genes controlling these processes in the distinct subgroups, we observed consistent reduction in methylation at CpG sites governing expression of *WNT5A* in *ALK* fusion cases (Figure 4D), *STAT1* in *NTRK* fusion cases (Figure 4E) and *TP63* in fusion-negative samples (Figure 4F) (Supplementary Table S5). This resulted in differential protein expression as assessed by multi-labeled immunofluorescence with antibodies directed against these targets, with representative examples shown for WNT5A and STAT1 in *ALK*-fusion (Figure 4G) and *NTRK*-fusion (Figure 4H) cases respectively. Using a NanoString assay for the 30 most differentially methylated genes between subgroups, we were able to distinguish ALK- / NTRK- fusion positive and -negative subgroups in a series of 21 infant HGG for which we had sufficient material (Figure 4I). Notably, we did not observe TP63 protein expression in any of our samples, although differential overexpression of the transcript was observed for fusion-negative cases.

Histological examination of those tumors classified as IHG revealed highly cellular astrocytic tumors with cells arranged in uniform sheets throughout the section (Supplementary Figure S6A,B,C). Cytologically, spindled nuclei (Supplementary

Figure S6D), an occasional ganglion cell component (Supplementary Figure S6E), or gemistocyte-like cells (Supplementary Figure S6F) could be seen either focally or throughout the tumor. Tumors frequently showed a superficial hemispheric location often involving the meninges, and had a well-defined border with adjacent normal brain. Palisading necrosis (Supplementary Figure S6G), microvascular proliferation and mild-moderate nuclear pleomorphism were almost universally seen. In some cases, a more nodular architecture was observed (Supplementary Figure S6H,I). Rarely, some showed less cellularity (Supplementary Figure S6J), and mineralisation, calcification or xanthomatous change could be observed (Supplementary Figure S6K). Consistent with these features, 67/80 (84%) of IHG cases were originally diagnosed as a high-grade glioma, although a variety of other diagnoses were included in the original pathology reports (Supplementary Figure S6L). A summary of the histological findings is given in Supplementary Table S6, with no statistically significant difference of features assessed between fusion-positive and-negative subgroups. The number of mitoses observed was highly variable, and proliferation as assessed by Ki67 staining highlighted cases presenting with both frequent (Supplementary Figure S6M) and sparsely positive nuclei (Supplementary Figure S6N). There was a significantly elevated Ki67 index in *NTRK* fusion-positive compared to fusion-negative IHG cases (p=0.0479, t-test), though not for *ALK* (p=0.3622, t-test) (Supplementary Figure S6O). Notably, the *NTRK* (median=22.5) and *ALK* (median=15.6) fusion-positive indices are at the upper end of values reported (38) for older patients with grade IV (median=15.8) and grade III (median=11.8) glioblastomas and anaplastic astrocytomas, with fusion-negative cases (median=5.6) closer to grade II astrocytomas (median=3.0).

Generation and pre-clinical testing of an ALK fusion-driven in vivo model

To assess the tumorigenic potential of the most commonly detected *ALK* gene fusion variant (*PPP1CB:ALK*) in a model system, we attempted to generate an *in vivo*

model using two complementary somatic gene transfer-based methods (RCAS/Ntv-a viral gene transfer and *in utero* electroporation (IUE)) (Figure 5A). When using the RCAS approach with injection of cells producing *PPP1CB:ALK*-containing virus at p0 on a *Cdkn2a* null background, tumor formation was rare (2/19 mice), and only after 300 days. By contrast, *in utero* electroporation at E14.5 with *PPP1CB:ALK* alone was able to generate consistent tumour formation with 100% penetrance, albeit with a relatively long latency of more than 250 days. Although not commonly found in the human disease, when combined with CRISPR/Cas9-mediated knockout of either *Trp53* or *Cdkn2a* for practical purposes, we observed highly efficient tumor formation with a median survival of 32 and 52 days, respectively (Figure 5B). *PPP1CB:ALK* mice +/- Cdkn2a-ko gave rise to tumors which reflected the human setting, including the typical foci of palisading necrosis, mitotic activity, glial cytology and/or clear astrocytic differentiation (Supplementary Figure S7A). All tumors would be classified as high-grade astrocytomas or glioblastomas. Staining for the HA epitope tag included at the C-terminus of the ALK fusion protein in the IUE/*Cdkn2a*-ko setting indicated widespread expression of the fusion protein, with invasion of individual tumor cells into the brain parenchyma (Supplementary Figure S7B).

To test the potential efficacy of targeted ALK inhibition in the context of this tumor model, we first dissociated tissue from a murine tumor into a single-cell suspension for growth in neurosphere (serum-free, non-adherent) conditions. Four different ALK inhibitors were then tested for *in vitro* growth inhibitory effects (crizotinib, ceritinib, alectinib, lorlatinib), representing different generations of inhibitor either approved for clinical use or currently in trials. Whilst all inhibitors showed a significant growth inhibitory effect at nanomolar concentrations (17) (Supplementary Figure S7C), there were differences in potency between the different compounds (Supplementary Table S7).

Due to its clear *in vitro* efficacy and reportedly good blood-brain barrier penetration (an important consideration for clinical translation for brain tumors), lorlatinib was chosen as the primary candidate for *in vivo* testing in our preclinical *ALK* fusion model. For this purpose, adult CD1 mice were allografted with short-term *in vitro*-cultured *PPP1CB:ALK*;*Cdkn2a-/-* cells and monitored for tumor growth using bioluminescence imaging (BLI). At the start of treatment (14 days after injection), mice were stratified into temozolomide (standard chemotherapy), vehicle control or lorlatinib arms, based on consecutive ranking (highest BLI signal to lorlatinib, 2nd highest to control, 3rd highest to temozolomide and so on). Whilst temozolomide was found to slow tumor growth in comparison with vehicle control, all tumors in these two treatment arms continued to grow. In contrast, all but one lorlatinib-treated animal displayed a significant reduction in BLI signal compared with the pre-treatment baseline (Figure 5C,D). This imaging response corresponded with a significant increase in survival in the lorlatinib-treated group compared with the two control arms ($p<0.0001$; although all tumors re-grew after stopping treatment after 28 days, with all mice ultimately needing to be sacrificed due to onset of tumor symptoms) (Figure 5E). No significant difference in body weight was observed between mice on the different treatment arms (data not shown), and the compounds were generally well tolerated. A similar experiment was performed using lorlatinib *versus* temozolomide in mice transplanted with cells from an ALK fusion-only mouse tumor. This also revealed a significant tumour regression (Supplementary Figure S7D) and survival increase with lorlatinib ($p=0.004$, log-rank test), with one animal showing prolonged survival at last follow-up, 8 months post injection (~6 months after end of treatment) (Supplementary Figure S7E). Overall, these findings provide a strong pre-clinical rationale for the potential use of targeted ALK inhibition in a clinical setting. For one of the cases in our study, DKFZ_INF_307, we have been able to demonstrate this directly. Here, a 1 month old boy underwent a left craniotomy with gross total resection, and was diagnosed as glioblastoma (WHO grade IV). He

underwent successive rounds of HIT SKK / ACNS and temozolomide chemotherapy, eventually showing progressive disease after both. He was found to have a *MAD1L1:ALK* fusion and was started on ceritinib, resulting in stable residual disease for nearly two years to date (Figure 5F).

Patient-derived models and clinical experience with NTRK inhibitors

Finally, we explored the utility of treating RTK fusion-positive infant gliomas with targeted inhibitors. We established two primary patient-derived cell cultures from infant glioma specimens with either *TPM3:NTRK1* or *ETV6:NTRK3* fusions (Figure 6A) and compared their *in vitro* sensitivities to three small molecule inhibitors of TrkA/B/C with two fusion-negative paediatric glioma cultures (Figure 6B). *NTRK* fusion-positive cells were more sensitive to entrectinib, crizotinib and milciclib, with differential sensitivities ranging from 2-9 fold over fusion-negative cells ($p=0.0253$, crizotinib; $p=0.0786$, entrectinib; $p=0.0141$, milciclib) (Supplementary Table S7), and reduction in downstream signalling via phospho-Akt and phospho-Erk (Supplementary Figure S7F). The infant glioma models were not tumorigenic after multiple orthotopic implantation experiments in immunodeficient mice, precluding *in vivo* assessment (data not shown).

Clinical treatment with Trk inhibitors was given to two patients in our cohort with *ETV6:NTRK3* fusions. The first case, OPBG_INF_035 was a girl diagnosed with a large frontal mass at 36 weeks' gestation (Figure 6C). It was a large, heterogenous mass with solid, cystic and haemorrhagic components. A biopsy was performed after birth and it was diagnosed histologically as a glioblastoma (WHO grade IV). The child subsequently received chemotherapy (methotrexate, vincristine, etoposide, cyclophosphamide, thiotepa) before undergoing a subtotal resection 3 months later. An *ETV6:NTRK3* fusion was identified in the DNA from both the biopsy and resection specimens, and four months post-surgery, the child was commenced on crizotinib.

An MRI scan performed after 9 months of treatment with crizotinib showed a 56% reduction in the size of the remaining solid component of the tumor compared to the post-surgery MRI scan (RANO criteria size reduction of >50% and stable). After an additional 3 months treatment with larotrectinib, the remaining solid component showed a further reduction in size now reaching 73% (Supplementary Figure S8A). Clinically, the child remains well. The second patient, MSKC_INF_006, presented with a generalized seizure aged 11 months (Figure 6D). An MRI scan revealed a pontine mass with central haemorrhage. The child underwent surgery and a gross total resection was achieved. Histologically the tumor was diagnosed as a low grade neuroepithelial neoplasm. The child developed a recurrence, at which point vincristine and carboplatin were commenced and a complete response was achieved. However, the tumor progressed two years after the original resection; a further gross total resection was achieved and the child treated with larotrectinib after an *ETV6:NTRK3* fusion was identified, with the aim of preventing further recurrence. To date, the child remains well with no evidence of recurrence after 12 months of treatment.

Notably, the patients from whose tumors our primary cell lines were derived have both only received surgery to date, and remain well. QCTB_INF_R077 was diagnosed with a tumor in the left fronto-parietal lobe *in utero* and underwent biopsy and subsequent resection shortly after birth . Histologically, the tumor was reported as a primary neuro-epithelial tumor. The child was not treated with any adjuvant therapy. At 5.5 years old, there has been no progression or relapse and the child has stable disease (Supplementary Figure S8B). The second patient, QCTB_INF_R102 aged 8 months, presented with a tumor in the left temporal lobe aged 8 months. He subsequently received a gross-total resection, with the tumor diagnosed as a ganglioglioma (WHO grade I). He also did not receive any adjuvant therapy post

resection and is currently 4 years old and remains stable under regular surveillance (Supplementary Figure S8C).

In summary, diffuse infant gliomas represent distinct disease entities marked by characteristic clinicopathological profiles and in most cases clinically actionable gene fusions (Figure 7).

Discussion

Malignant glioma presenting in infancy represents a specific clinical challenge, involving diagnostic uncertainty and a hesitancy to aggressively treat given the reported superior outcomes compared with older children, coupled with the high risk of neurocognitive deficits (39). This is compounded by a lack of biological understanding due to the rarity of these tumors. The present international collaborative study brings together the largest collection of tumors originally reported as high grade or diffuse gliomas in this age group, by contrast with another recent multi-institutional study which was predominantly comprised of low grade tumours (17). Our study uniquely includes methylation and gene expression data, and allows for refinement of subgroups within the malignant spectrum of disease with important clinical management implications; we also present experience of clinical responses with targeted agents even after progression on standard chemotherapies.

A first key finding relates to the difficulty of differential diagnoses in these very young children, with ~10% cases unequivocally classifying as other tumor entities on the basis of methylation profiling (40) or the presence of pathognomonic gene fusions (36), even after discounting mis-diagnosed or mis-assigned pilocytic astrocytomas. Often this uncertainty is reflected in the original pathology report, with atypical features highlighted. However, the highly heterogeneous nature of high grade glial tumors provides for a broadly inclusive category in the current WHO classification, which in many cases may result in what is considered to be a relatively uncontroversial histological diagnosis despite widely varying morphologies. Similarly, combined genetic and epigenetic analyses reveal a third of remaining cases to be biologically identical to known high or low grade glioma subtypes, with substantially different prognoses reflective of the known clinical course of the relevant tumor categories. Together, these data make the important points that histopathologic evaluation alone is insufficient to predict outcome, and that high grade gliomas

predominantly occuring in older childhood may also present in the infant population with little survival benefit from standard treatment protocols.

After these exclusions, there remains what we define as an intrinsic set of infant gliomas, which are largely restricted to the cerebral hemispheres and occur in the youngest patients, usually under 12 months old. These patients, despite more than three-quarters unequivocally reported as WHO grade III or IV astrocytoma, have an overall survival more akin to lower grade tumors, yet lack the key molecular features of both HGG and LGG. They appear to form a biological continuum of disease between the recognized MAPK-driven desmoplastic lesions (DIGG/DIA), which may respond clinically to targeted *BRAF* V600E inhibitors, even after previous chemotherapy (41), and a novel assignation of diffuse infant hemispheric glioma. This latter end of the spectrum is strikingly defined by nearly two-thirds of tumors harboring fusions in genes encoding the receptor tyrosine kinases *ALK*, *NRTK1/2/3*, *ROS1* and *MET*. Although structural variants involving these genes within the age group have been described in case reports (27-35) and a recent larger study (n=29) (17), the current report represents a uniquely powerful study of these rare tumors, by accumulating a series of 82 infant cases with RTK fusions with full methylation profiles.

Molecularly, these events included interstitial microdeletions such as those at chromosome 2p23 resulting in the fusion of *CCDC88A or PPP1CB* and *ALK* (17,34) and at 6q21 fusing *ROS1* and *GOPC* (previously known as *FIG*, and originally described in an adult GBM cell line (42)); additional focal DNA copy number losses targeted *MET* at 7q31 (43). There were multiple instances of inter-chromosomal copy number gains fusing *ALK* to a series of novel partners, including *MAD1L1* (7p22), *ZC3H7A* (16p13), *MSI2* (17q22), *SYNDIG1* (20p11) and *SPECC1L* (22q11), as well as the intra-chromosomal *EML4:ALK* fusion that is well-characterized in non-small

cell lung cancer and others (44). The *NTRK* genes had a variety of inter-chromosomal partners, with around half of cases marked by a DNA copy imbalance at either locus. Notably, *NTRK2* fusions (also described in LGG (25,26,45)) were largely found in tumors classifying as other glioma subtypes, as were the previously described *FGFR:TACC* fusions (46).

Histopathologically, within the context of HGGs, certain common features of the intrinsic infant hemispheric gliomas could be recognized. Cases tended to have a relatively uniform architecture, with marked pleomorphism. There was an enrichment of gemistocytic-like cells, as has been reported for a case with *ZCCHC8:ROS1* fusion (29); a predominance of spindle cell differentiation, reminiscent of mesenchymal tumors with *NTRK* fusions (47), and also described in an *ETV6:NTRK3* infant glioma (35). Our *NTRK* fusion cases in the present study clustered distinctly from *ETV:NTRK3*-positive infantile fibrosarcoma and congenital mesoblastic nephroma, however, suggesting a distinct origin. Several cases also had ependymal differentiation, consistent with two cases with *ALK* fusions (*KTN1:ALK* and *CCDC88A*:*ALK)* reported as not easily fitting the established WHO brain tumor entities (34). Notably, *CCDC88A*:*ALK* cases have been reported clinically as both low- and high- grade glioma, however the same study found tumours generated by overexpressing the fusion in xenografted immortalized human astrocytes to have a high proliferative index, glial marker expression and pseudopallisading necrosis (17), suggestive of high grade lesions in common with our *in utero* electroporation modelling approach. A further case report described a *KIF5B:ALK* fusion in an infant with microglial proliferation, spindle cells with scattered mitotic figures, and a mixed inflammatory infiltrate of scattered lymphocytes, plasma cells and eosinophils, indicating potential microglioma or gliofibroma (31). The recognition of tumors in this series that biologically resemble DIGG/DIA (WHO grade I) is compatible with their histology, in that some cases have been described as presenting with a poorly

differentiated component (39). The case with *ZCCHC8:ROS1* fusion was also described to display a cellular element within a fusocellular desmoplastic component (29), and we noted focal ganglion cells in our series. However, despite these differences, it is still not possible at the present time to define clear histology-only criteria which can reliably distinguish between these molecularly-defined intrinsic infant tumors and other glioma subtypes in the same age group.

The presence of recurrent *ALK/NTRK/ROS1/MET* fusions represent clearly targetable alterations, in common with subgroups of adult epithelial tumors (48,49), and their identification through screening approaches and routine diagnostic sequencing panels (50-53) makes them amenable to selection for clinical trials despite their rarity. The distinct morphological variants, the restricted spatial and temporal patterns of presentation, and the specificity of oncogenic events largely in the absence of other mutations or large-scale chromosomal rearrangements suggests an exquisite developmental susceptibility for transformation which would account for this rare subgroup of tumors.

Multiple *ALK* partners are associated with synapse formation and activity (*CCDC88A, HIP1, SYNDIG1*), neuronal cytoskeletal reorganisation (*CCDC88A, SPECC1L*) and microtubule assembly (*MAP2, PRKAR2A, EML4*), as well as PI3K/MAPK signalling (*PPP1CB, CCDC88A, SPECC1L*) and cell cycle progression (*MAD1L1*) (54-62). Thus in addition to the activated kinase activity of the ALK receptor itself, these fusions likely disrupt key regulatory processes in neurodevelopment, as exemplified by the differential methylation of genes controlling these processes we observed. The most common *ALK* fusion, *PPP1CB:ALK,* was found to be tumorigenic when introduced in prenatal, though largely not postnatal mice, further demonstrating the importance of developmental context associated with the oncogenicity of these alterations.

*AL*K fusion-positive tumors were found to be sensitive to targeted ALK inhibition *in vitro* and *in vivo*, resulting in tumor shrinkage and extension of survival in the latter in contrast to the standard chemotherapeutic agent temozolomide. Excitingly, this experience was mirrored in the clinic, whereby a child diagnosed at 1 month old experienced stable disease for nearly two years on targeted therapy after progressing on two successive chemotherapy protocols, including temozolomide. Critically, *NTRK* fusion cases were also found to respond to targeted inhibitors in patient-derived models *in vitro* as well as in children treated clinically, in common with isolated reported cases (35), whereby for example a 3-year-old girl who had failed multiple therapies including chemotherapy and radiotherapy showed near total resolution of primary and metastatic lesions after treatment with larotrectinib. If validated in larger trials, such agents may represent attractive options in order to spare the long-term sequalae of chemotherapy and radiotherapy, whilst maintaining the generally good prognosis of these patients (27,30,33).

Despite the frequency of alterations identified, not all of the intrinsic infant gliomas were found to harbor RTK fusions. These fusion-negative cases (at least on the basis of the platforms used in this study) had a lower proliferation index compared to *NTRK*-positive cases, but a worse prognosis under standard treatment. Although we could identify no apparent recurrent genetic driver of this subgroup, even with whole genome sequencing of a subset of cases, there were clear epigenetic differences compared to fusion-positive cases, with dysregulated gene networks associated with the regulation of stem cell pluripotency, plausibly suggesting an immature progenitor cell phenotype for these genetically bland lesions. By contrast, *NTRK*-fusion cases were associated with an embryonic, neuronal developmental programme, and *ALK*-fusion cases with later AMPA-receptor synaptic plasticity signatures.

Further work is needed to explore all intrinsic infant glioma subgroups, in particular the fusion-negative cases. However, it is clear that these tumors harbor unique biology with associated clinicopathological differences, and should no longer be diagnosed or treated in the same way as their older counterparts. Maximal safe surgical resection remains the aim of treatment, regardless of subtype (17). However, our study has shown that RTK fusions can be found across all subgroups (although more frequently seen in the IHG group) and so screening (initially via copy number profiling with subsequent validation) will help to identify patients who may be eligible for targeted therapy or clinical trials.

Author contributions

MCl, AMac, BI, DWE, DTWJ, TSJ and CJ designed the study, analysed data, and wrote the manuscript. LHi, JP, RGT, TBa, KMK, CR, MM, SCr, JK, US, UK, DK, MSi, LBr, AJM, LD, SA-S, CCa, BZ, CCh, MSn, IJD, SWG, TM, CH, ISl, RP, H-KN, SCa, BFK, MP, SG, MW, LBa, TKO, PB, MF, JCr, MCa, MKa, MKR, JS, ME, WD, KK, MvB, TP, FA, PHD, AK, DS, MZ, OW, DC, TBl, CM, EM, FDC, GSC, SB, ASM, TEGH, SL, MAK, CMK, MT, MJC, DSZ, KA, DHa, FC, LM, FS, AvD, SMP, SJB, AMas, AC and MV provided cases, data and/or clinical annotation. SN, ISt, BCW, EI, ST, DAS, DMC, VM, AB, LHo, DS, AV, ARF, AA, JCh, MKr, MD, KH, JD, WO, JW MH, RN, JKRB, SPR, DHu, PP, and SP carried out experiments and data analysis. All authors reviewed and approved the final manuscript.

Methods

Cases

All patient samples included were classified as gliomas (WHO grade II, III or IV) aged <4 years old (including congenital cases) from all CNS locations (including spinal tumors). Cases were excluded if they had been diagnosed as a pilocytic astrocytoma with a known *BRAF* fusion or mutation. Ependymal, embryonal, mesenchymal and germ cell tumors were also excluded. Samples were received from national (Great Ormond Street Hospital, London, n=33; King's College Hospital, London, n=21; University Hospitals Bristol, n=9; Newcastle Royal Infirmary, n=6; St George's Hospital, London, n=4) and international collaborators (German Cancer Research Center (DKFZ), n=86; Ospedale Pediatrico Bambino Gesù, n=37; St Jude Children's Research Hospital, Memphis, n=17; Memorial Sloan Kettering Cancer Center, New York, n=6; Queensland Children's Tumor Bank, Brisbane, n=5; Universitätsklinikum Hamburg-Eppendorf, n=5; Children's Cancer Institute, Sydney, n=2; Children's Hospital of Wisconsin, n=2; Emory University Hospital, Atlanta, n=1; St. Petersburg Hospital No. 6, n=1; Wake Forest School of Medicine, Winston-Salem, n=1; The Chinese University of Hong Kong, n=1; Children's National Medical Centre, Washington DC, n=1; Chaim Sheba Medical Center, Tel Aviv, n=1; Oregon Health & Science University, Portland, n=1; University of Ljubljana, n=1). Where possible an H&E slide, 10 unstained sections, formalin-fixed paraffin-embedded (FFPE) tissue rolls, or frozen tissue was provided for each case. In some cases, data alone was provided. A total of 241 cases were entered into the study. Eight cases from King's College and St George's Hospital London (8), and ten cases from St Jude Children's Hospital Memphis (9) have been previously published. All patient samples were collected under full Research Ethics Committee approval at each participating centre.

Nucleic acid extraction

DNA was extracted from frozen tissue by homogenisation prior to following the DNeasy Blood & Tissue kit protocol (QIAGEN, Hilden, Germany). DNA was extracted from formalin-fixed, paraffin-embedded (FFPE) pathology blocks after manual macrodissection using the QIAamp DNA FFPE tissue kit protocol (QIAGEN). Concentrations were measured using a Qubit fluorometer (Life Technologies, Paisley, UK). RNA was extracted by following the RNeasy Mini Kit protocol (QIAGEN), and quantified using a Nanodrop 2000 Spectrophotomer (Thermo Scientific).

Methylation profiling

The quantity and quality of DNA varied between cases with FFPE samples yielding less (range for FFPE: 11.0 – 2960.0ng, range for fresh frozen: 211.0 - 5358.0ng). Methylation analysis was performed when >150ng of DNA was extracted, using either Illumina 450K or EPIC BeadArrays at DKFZ (Heidelberg), University College London (UCL) Great Ormond Street Institute of Child Health or St. Jude Children's Research Hospital. Data from Illumina 450k or EPIC arrays was pre-processed using the minfi package in R (v11b4). DNA copy number was recovered from combined intensities using the conumee package. The Heidelberg brain tumor classifier (molecularneuropathology.org) (40) was used to assign a calibrated score to each case, associating it with one of the 91 tumor entities which feature within the current classifier (v4). Clustering of beta values from methylation arrays was performed based upon correlation distance using a ward algorithm. DNA copy number was derived from combined $\log_2$ intensity data based upon an internal median processed using the R packages minfi and conumee to call copy number in 15,431 bins across the genome. Gene ontology analysis of differentially methylated regions was carried out using methylGSA (rdrr.io/bioc/methylGSA/), adjusting the number of CpGs for each gene by weighted resampling and Wallenius non-

central hypergeometric approximation in methylgometh (63). Ontology networks were constructed using ShinyGO (bioinformatics.sdstate.edu/go/).

Fusion panel

A custom fusion panel consisting of 22 genes associated with fusions in paediatric brain tumors (*ALK, BCOR, BRAF, c11orf95, C19MC, CIC, ETV6, FGFR1-3, FOXR2, KIAA1549, MET, MN1, MYB, MYBL1, NTRK1-3, RAF, RELA, TPM3* and *YAP1*) was designed with a library of probes to ensure adequate coverage of the specified regions (Roche Sequencing Solutions) (64). Where available, 100-200ng of DNA was used for library preparation using KAPA Hyper and HyperPlus Kit (Kapa Biosystems) and SeqCap EZ adaptors (Roche). Following fragmentation, DNA was end-repaired, A-tailed and indexed adaptors ligated. DNA was amplified, multiplexed and hybridized using 1ug of the total pre-capture library DNA. After hybridisation, capture libraries were amplified and sequencing was performed on a MiSeq and NextSeq (Illumina). Quality control (QC), variant annotation, deduplication and metrics were generated for each sample. The raw list of candidates provided by Manta (https://github.com/Illumina/manta) were filtered for more than 2 reads covering both genes, common false positive base pairs (bp) positions/fusions outside of the capture set at both ends, common breakpoint/false positives within 10 bp, common false positive gene pairs, fusions within the same gene and homologous sequences greater than 10bp. Breakdancer was used to confirm all the breakpoints in all samples. Sequences either side of the break points were annotated to look for repetitive elements. A BLAT score was obtained to remove loci which were not uniquely mapped. Integrative Genomics Viewer (IGV) was used to view the fusions.

DNA and RNA sequencing

DNA was sequenced either as whole genome or captured using Agilent SureSelect whole exome v6 or a custom panel of 329 genes known to present in an unselected series of paediatric high grade glioma (8). Library preparation was performed using 50-200 ng of genomic DNA. Following fragmentation, DNA was end-repaired, A-tailed and indexed adapters ligated. DNA was amplified, multiplexed and hybridized using 1 µg of total pre-capture library. After hybridization, capture libraries were amplified and sequencing was performed on a NextSeq500 (Illumina) with 2 x 150bp, paired-end reads following manufacturer's instructions. Ribosomal RNA was depleted from 500-2000 ng of total RNA from FF and FFPE using NEBNext rRNA Depletion Kit. Following First strand synthesis and directional second strand synthesis resulting cDNAs were used for library preparation using NEBNext Ultra II Directional RNA library prep kit for Illumina performed as per the manufacturers recommendations. Exome capture reads were aligned to the hg19 build of the human genome using bwa v0.7.12 (bio-bwa.sourceforge.net), and PCR duplicates removed with PicardTools 1.94 (pcard.sourceforge.net). Single nucleotide variants were called using the Genome Analysis Tool Kit v3.4-46 based upon current Best Practices using local re-alignment around InDels, downsampling and base recalibration with variants called by the Unified Genotyper (broadinstitute.org/gatk/). Variants were annotated using the Ensembl Variant Effect Predictor v74 (ensembl.org/info/docs/variation/vep) incorporating SIFT (sift.jcvi.org) and PolyPhen (genetics.bwh.harvard.edu/pph2) predictions, COSMIC v64 (sanger.ac.uk/genetics/CGP/cosmic/), dbSNP build 137 (ncbi.nlm.nih.gov/sites/SNP), ExAc and ANNOVAR annotations. RNA sequences were aligned to hg19 and organized into de-novo spliced alignments using bowtie2 and TopHat version 2.1.0 (ccb.jhu.edu/software/tophat). Fusion transcripts were detected using chimerascan version 0.4.5a filtered to remove common false positives.

PCR / Sanger sequencing validation

PCR to validate fusion breakpoints was carried out using primers obtained from Integrated DNA Technologies (Illinois, USA). PCR products were cleaned using the ExoProStar S 20 (Sigma-Aldrich) and were sent for Sanger sequencing (DNA Sequencing and Services, University of Dundee, UK). Sequences were analysed manually with 4Peaks (Nucleobytes, Aalsmeer, Netherlands).

NanoString gene expression analysis

The top 30 genes with the most differentially methylated regions between *ALK*-fusion, *NTRK*-fusion and fusion negative cases were selected for an mRNA expression analysis using a custom nCounter platform and nDesign (NanoString, Seattle, WA, USA). Specimen RNA was mixed in hybridization buffer with CodeSets and hybridized overnight at 65°C. Samples wash reagents and imaging cartridge were processed on the nCounter Prep Station and imaged on the nCounter Digital Analyzer according to the manufacturer's instructions. Data were normalised with NanostringNorm v1.2.1 using variance stabilizing normalization (VSN). Heatmaps were made by clustering the median centred expression values or a correlation matrix based on Euclidean distance using a Ward D2 algorithm.

Immunofluorescence

Paraffin-embedded tissue sections were deparaffinized in three changes of xylene and ethanol. Heat-mediated antigen retrieval was performed (Dako S1699, pH 6.0) and tissue slides were permeabilized with 0.5% Triton X-100 solution for 10 min at room temperature and then blocked with appropriate serum according to the species of secondary antibody for 1 h at room temperature. For STAT1 staining (AHO0832, Invitrogen, 1:800), Alexa Fluor 488 Tyramide Super Boost Kit was used (B40941, Invitrogen) and antibody was incubated at 37 °C for 30 min. For WNT5A (MA5-

15502, Invitrogen, 1:800) and TP63 (39692, Cell signalling, 1:900) staining, samples were incubated at 37 °C for 30 min. Sample slides were then washed in PBS three times and incubated with DyLight 649 (DI-2649, Vector, 1:100) and Alexa Fluor 555 (A31572, Invitrogen, 1:300) -conjugated secondary antibodies for an hour at room temperature. Nuclei were counterstained with DAPI and samples mounted with Vectashield (H1000, Vector Laboratories) and examined using Zeiss Axio Scan.Z1 automated Fluorescence slide scanner.

Histology and immunohistochemistry

Histological review was undertaken according to the WHO Classification of Tumors of the Central Nervous System (2016) (65). Each case was reviewed blinded to the molecular features with a predetermined set of criteria to assess for the presence of histological features characteristic of gliomas such as necrosis, mitotic figures, stromal and astrocytic morphology. Any unusual features not previously associated with these tumors, including unusual nuclear morphology was noted. These features were then re-reviewed in the context of any molecular results identified. Immunohistochemistry for Ki67 (M7240, DAKO, 1:100) was carried out using pressure-mediated antigen retrieval and the Envision^{TM} detection system (DAKO K5007). Slides were mounted using Leica CV Ultra mounting medium, imaged using the high throughput-scanning microscope AxioScan Z1 and quantified using Definiens software.

Novel ALK fusion mouse model

A *PPP1CB:ALK* fusion construct was cloned into either an RCAS or a pT2K vector using RNA from a human glioma sample as template. After cDNA synthesis and PCR amplification, the ends of the product were cut with EcoRI and XhoI (for cloning into pT2K) or NotI and ClaI (for RCAS) and ligated into the target vector using the

Takara Ligation mixture (Clontech). Bacterial amplification and QIAprep® Spin Miniprep kit (QIAGEN) were performed according to manufacturer's instructions to isolate the cloned plasmid. The DNA was sequenced using Sanger Sequencing at GATC Biotech (Heidelberg, Germany) and protein expression was confirmed on Western Blot after transfection of DF-1 cells with the vector.

In utero electroporation: After confirming that the expression vector contained the right inserts, embryos of CD1 mice were injected with plasmid into the fourth ventricle and electroporated *in utero* at E14.5. The *PPP1CB:ALK* fusion plasmid was used alone or in combination with CRISPR guide RNAs against Cdkn2a. Due to the incorporated IRES-Luciferase reporter on the pT2K vector, mice with successful integration of the transgene could be assessed at postnatal day 3 using bioluminescence imaging on an IVIS imager (PerkinElmer). Mice were sacrificed upon first signs of tumor-related symptoms according to humane endpoint criteria. H&E and IHC staining was performed according to standard protocols on 3µm sections.

RCAS: Four days before the calculated birth date, early passage DF-1 fibroblasts for virus production were plated at 2-3x10^5 cells/ T25 flask in 5ml DMEM with 10% FCS + 1% Penicillin/Streptomycin (P/S) + 1% Glutamax at 5% CO_2 at 39°C. One day after, the cells were transfected with the RCAS construct as follows: 4µg of the RCAS plasmid was incubated in 200µl of room-temperature Optimem and 10µl FuGene transfection reagent. After a 15-minute incubation time, this mixture was slowly added to the settled DF-1 cells, mixed well by gently moving the flask and placed back in the incubator. An RCAS-GFP plasmid was always run in parallel in a separate flask to check for transfection success. On the day of birth, the transfected DF-1 cells were harvested using 10x Trypsin-EDTA and counted using the automated cell counter TC20™. 4x10^5 cells in 1µl were used for injection into

newborn Ntv-a;Cdkn2a$^{-/-}$;Pten$^{fl/fl}$ pups at p0. The required amount of cells, depending on the size of the litter, was eluted in DMEM culture medium. The pups were taken out of the cage in a sterile hood and injected into the striatum with 1µl of the DF-1 cell solution using a 10µl Hamilton syringe. Mice were sacrificed upon first signs of tumor-related symptoms according to humane endpoint criteria. All animal protocols were approved by the relevant authority (Regierungspräsidium Karlsruhe) under registration numbers G-212/16 and G-168/17.

In vitro culture and compound testing of murine tumor cells

Murine ALK fusion-positive tumors were dissected immediately post mortem, mechanically dissociated and then filtered through a 40µm cell strainer. Cells were then plated *in vitro* in 10cm dishes and grown as spheres in a 1:1 mix of Neurobasal-A and DMEM/F-12 media containing 1% 1M HEPES buffer solution, 1% 100mM sodium pyruvate MEM, 1% 10mM MEM non-essential amino acids solution, 1% GlutaMAX and 1% antibiotic-antimycotic supplemented with 2% B27, 2µg/ml heparin solution, 10ng/ml H-PDGF-AA, 20ng/ml recombinant human bFGF and 20ng/ml recombinant human EGF. For splitting, cells were dissociated with Accumax at 37°C for 5 minutes.

For *in vitro* drug testing, primary sphere culture cells were plated at 1x10^4 cells/well in 80µl growth factor-containing medium/well in 96-well plates. Triplicates per drug concentration (20µl total volume for each) were added 24 hours after seeding the cells. The drug concentrations ranged between 1nM and 30µM. Corresponding DMSO concentrations were plated as controls, to which the treated wells were normalized. The ALK inhibitors crizotinib, alectinib, ceritinib and lorlatinib were used. All compounds were purchased from Selleck Chemicals and initially diluted in DMSO to either a 10mM or 1mM stock, which were stored at -80°C. A CellTiter-Glo assay (Promega) was used as a readout of compound efficacy. This assay was conducted

72 hours after drugs were added to the cells. For this purpose, 50µl of CellTiter-Glo substrate were added to each well using a multichannel pipette, and plates were incubated for 15 minutes whilst shaking in the dark. After that time, the luminescence signal per well was measured using a Mithras LB940 microplate reader. The respective DMSO control value was subtracted from the drug's value to normalize the readout. The GI_{50} curves show the mean ± SD of the triplicates per condition measured. Representative results from duplicate experiments are shown.

Western blot analysis

Cells were incubated in complete media with vehicle or increasing concentrations of Entrectinib (0.1, 1, 10 µM) and protein was collected 4h post-treatment. Samples were lysed by using lysis buffer (CST) containing phosphatase inhibitor cocktail (Sigma, Poole, UK) and protease inhibitor cocktail (Roche Diagnostics, Burgess Hill, UK). Following quantification using Pierce BCA Protein Assay Kit (Thermo Fisher), cell extracts were loaded for Western blot analysis. Membranes were incubated with primary antibody (1:1000) overnight at 4 °C, and horseradish peroxidase secondary antibody (Amersham Bioscience, Amersham, UK) for 1 h at room temperature. Signal was detected with ECL Prime western blotting detection agent (Amersham Biosciences), visualised using Hyperfilm ECL (Amersham Biosciences) and analysed using an X-ray film processor in accordance with standard protocols. Primary antibodies used were phospho-AKT (Ser473) (CST# 4060), phospho-p44/42 (Thr202/Tyr204) (CST#4370), AKT (CST#9272), p44/42 (CST#9102), GAPDH (CST#2118), all Cell Signalling (Danvers, MA, USA).

In vivo compound testing

To test the effectiveness of ALK inhibition *in vivo*, 6 week old CD1 mice were intracranially allografted with 5x 10^5 mouse *PPP1CB:ALK* tumor cells (see above) in order to give a more standardized latency of tumor formation and to ensure avoid

having to administer treatment to very young animals. The chosen inhibitor was lorlatinib based on the *in vitro* results, as well as HCl and temozolomide as vehicle control and standard-of-care, respectively. Dosing and treatment schedules were as previously described (66). Tumor growth was monitored using bioluminescence imaging on an IVIS imager (PerkinElmer). The tumors were allowed to develop for two weeks before animals were stratified into three treatment groups based on their luciferase signal (rank 1, 4, 7 etc. being assigned to lorlatinib, rank 2, 5, 8 etc. to temozolomide, and rank 3, 6, 9 etc. to vehicle control). Animals were monitored daily for symptoms or abnormal behavior and weighed three times a week, and were sacrificed upon first signs of tumor-related symptoms according to humane endpoint criteria.

Novel patient-derived NTRK fusion models

Each cell culture was initiated using the following method; tissue was first minced using a sterile scalpel followed by enzymatic dissociation with LiberaseTL for 10 min at 37°C. Cells were grown under stem cell conditions, as two-dimensional (2D) adherent cultures on laminin and laminin/fibronectin. Cells were cultured in a serum-free medium, Tumor Stem Media (TSM) consisting of 1:1 Neurobasal(-A), and DMEM:F12 supplemented with HEPES, NEAA, Glutamaxx, sodium pyruvate and B27(-A), human bFGF (20ng/mL), human-EGF (20ng/mL), human PDGF-AA (10ng/mL) and PDGF-BB (10ng/mL) and heparin (2ng/mL). Control lines QCTB-R006 (9.5 years, male, frontal lobe GBM, wildtype) and QCTB-R059 (10.4 years, female, thalamic, *H3F3A*K27M mutant) were also grown as adherent cultures (laminin and laminin-fibronectin). Cells were dissociated enzymatically with accutase and counted using a Beckman-Coulter ViCell cell viability analyser.

For intracranial implantation, all experiments were performed in accordance with the local ethical review panel, the UK Home Office Animals (Scientific Procedures) Act

1986, the United Kingdom National Cancer Research Institute guidelines for the welfare of animals in cancer research and the ARRIVE (Animal Research: Reporting *In Vivo* Experiments) guidelines (67,68). Single cell suspensions were obtained immediately prior to implantation in NOD.Cg-*Prkdc*^{scid} *Il2rg*^{tm1Wjl}/SzJ (NSG) mice (Charles River, UK). Animals were anesthetized with intraperitoneal ketamine (100mg/kg)/xylazine(16mg/kg) and maintained under 1% isoflurane (0.5L/min). Animals were depilated at the incision site and Emla cream 5%(lidocaine/prilocaine) was applied on the skin. A subcutaneous injection of buprenorphine (0.03mg/Kg) was given for general analgesia. The cranium was exposed via midline incision under aseptic conditions, and a 31-gauge burr hole drilled above the injection site. Mice were then placed on a stereotactic apparatus for orthotopic implantation. The coordinates used for the cortex were x=-2.0, z=+1.0, y=-2.5mm from bregma. 300,000 cells in 5µL were stereotactically implanted using a 25-gauge SGE standard fixed needle syringe (SGE™ 005000) at a rate of 2µl/min using a digital pump (HA1100, Pico Plus Elite, Harvard Apparatus, Holliston, MA, USA). At the completion of infusion, the syringe needle was allowed to remain in place for at least 3 minutes, and then manually withdrawn slowly to minimize backflow of the injected cell suspension. An intraperitoneal (IP) injection of the reversing agent atipamezole (1mg/kg) diluted in Hartmann's solution for rehydration was administered. Mice were monitored until fully recovered from surgery and given Carprofen (analgesia) in a gel diet for 48 hours post-surgery. Mice were weighed twice a week and imaged by ^{1}H magnetic resonance imaging (MRI) on a horizontal bore Bruker Biospec 70/20 system (Ettlingen, Germany) equipped with physiological monitoring equipment (SA Instruments, Stony Brook, NY, USA) using a 2cm x 2cm mouse brain array coil. Anaesthesia was induced using 3% isoflurane delivered in oxygen (1l/min) and maintained at 1-2%. Core body temperature was maintained using a thermo-regulated water-heated blanket.

In vitro compound testing of patient-derived cells

Cells were seeded (3000-5000 cells per well) into laminin or laminin-fibronectin coated 96-well plates and treated with different Trk inhibitors at concentration ranging from 0 to 20uM for 8 days. The drugs used were entrectinib (RXDX-101, Selleckchem), crizotinib (PF-02341066, Selleckchem) and milciclib (PHA-848125, Selleckchem). Each assay was performed in three independent biological replicates of three technical replicates each. Cell viability was assessed with Cell Titer-Glo using a FLUOstar Omega plate reader (BMG, LABTECH). Data was analysed and IC50 values were calculated using GraphPad Prism software.

Statistics

Statistical analysis was carried out using R 3.5.0 (www.r-project.org) and GraphPad Prism 7. Categorical comparisons of counts were carried out using Fishers exact test, comparisons between groups of continuous variables employed Student's t-test or ANOVA. Univariate differences in survival were analysed by the Kaplan-Meier method and significance determined by the log-rank test. All tests were two-sided and a *p* value of less than 0.05 was considered significant.

Data availability

All newly generated data have been deposited in the European Genome-phenome Archive (www.ebi.ac.uk/ega) with accession number EGAS00001003532 (sequencing) or ArrayExpress (www.ebi.ac.uk/arrayexpress/) with accession numbers E-MTAB-7802 and E-MTAB-7804 (methylation arrays). Curated gene-level copy number, mutation data and RNAseq data are provided as part of the paediatric-specific implementation of the cBioPortal genomic data visualization portal (pedcbioportal.org).

Acknowledgments

This work was supported by the CRIS Cancer Foundation and the INSTINCT network funded by The Brain Tumour Charity, Great Ormond Street Children's Charity and Children with Cancer UK, Cancer Research UK. The authors acknowledge NHS funding to the National Institute for Health Research Biomedical Research Centre at The Royal Marsden and the ICR, the NIHR Great Ormond Street Hospital Biomedical Research Centre, research nurse funding by the Experimental Cancer Medicines Centre (ECMC) Paediatric Network, as well as CRUK support to the Cancer Imaging Centre at the ICR and Royal Marsden in association with the MRC and Department of Health (England) (C1060/A16464). Further funding support was provided by the German Children's Cancer Foundation (DKKS, project "MNP2.0 – Improving the Diagnostic Accuracy of Pediatric Brain Tumors", and support for the German Brain Tumor Reference Center of the DGNN, grant 2014.17) and the PedBrain Tumour Project contributing to the International Cancer Genome Consortium, funded by German Cancer Aid (109252) and by the German Federal Ministry of Education and Research (BMBF, grant #01KU1201A), and the DKFZ-MOST Cooperation Program. We would like to thank Laura von Soosten (DKFZ) for technical assistance and Richard Buus (ICR) and the Breast Cancer Now NanoString facility for conducting the NanoString gene expression profiling. The authors thank Brain UK for provision of cases and clinical information. The authors thank the Cure Brain Cancer Foundation, Australian Lions Childhood Cancer Research Foundation and Lions Club International Foundation (LCIF). Some of the results are in part based upon data generated by Lions Kids Cancer Genome Project (LKCGP) Partners. The authors thank the German Cancer Research Center (DKFZ) Genomics and Proteomics Core Facility and the Hartwell Center at St. Jude Children's Research Hospital for technical support. The authors acknowledge funding from the American, Lebanese and Syrian-Associated Charities (ALSAC). The Queensland Children's Tumour Bank is funded by the Children's Hospital Foundation

(Queensland). This work was funded in part by the Marie-Josée and Henry R. Kravis Center for Molecular Oncology and the National Cancer Institute Cancer Center Core Grant No. P30-CA008748. We gratefully acknowledge the members of the Memorial Sloan Kettering Molecular Diagnostics Service in the Department of Pathology. MSn acknowledges funding from the Friedberg Charitable Foundation, the Making Headway Foundation and the Sohn Conference Foundation. AK is supported by the Helmholtz Association Research Grant (Germany). MV is a CwCUK Fellow (grant number 16-234). SJB acknowledges funding support from the NIH (CA096832).

References

1. Jones C, Perryman L, Hargrave D. Paediatric and adult malignant glioma: close relatives or distant cousins? Nat Rev Clin Oncol **2012**;9(7):400-13 doi 10.1038/nrclinonc.2012.87.

2. Schwartzentruber J, Korshunov A, Liu XY, Jones DT, Pfaff E, Jacob K*, et al.* Driver mutations in histone H3.3 and chromatin remodelling genes in paediatric glioblastoma. Nature **2012**;482(7384):226-31 doi 10.1038/nature10833.

3. Wu G, Broniscer A, McEachron TA, Lu C, Paugh BS, Becksfort J*, et al.* Somatic histone H3 alterations in pediatric diffuse intrinsic pontine gliomas and non-brainstem glioblastomas. Nat Genet **2012**;44(3):251-3 doi 10.1038/ng.1102.

4. Jones C, Baker SJ. Unique genetic and epigenetic mechanisms driving paediatric diffuse high-grade glioma. Nat Rev Cancer **2014**;14(10) doi 10.1038/nrc3811.

5. Sturm D, Witt H, Hovestadt V, Khuong-Quang DA, Jones DT, Konermann C*, et al.* Hotspot mutations in H3F3A and IDH1 define distinct epigenetic and biological subgroups of glioblastoma. Cancer Cell **2012**;22(4):425-37 doi 10.1016/j.ccr.2012.08.024.

6. Bouffet E, Larouche V, Campbell BB, Merico D, de Borja R, Aronson M*, et al.* Immune Checkpoint Inhibition for Hypermutant Glioblastoma Multiforme Resulting From Germline Biallelic Mismatch Repair Deficiency. J Clin Oncol **2016**;34(19):2206-11 doi 10.1200/JCO.2016.66.6552.

7. Shlien A, Campbell BB, de Borja R, Alexandrov LB, Merico D, Wedge D*, et al.* Combined hereditary and somatic mutations of replication error repair genes result in rapid onset of ultra-hypermutated cancers. Nat Genet **2015**;47(3):257-62 doi 10.1038/ng.3202.

8. Mackay A, Burford A, Carvalho D, Izquierdo E, Fazal-Salom J, Taylor KR*, et al.* Integrated Molecular Meta-Analysis of 1,000 Pediatric High-Grade and Diffuse Intrinsic Pontine Glioma. Cancer Cell **2017**;32(4):520-37 e5 doi 10.1016/j.ccell.2017.08.017.

9. Wu G, Diaz AK, Paugh BS, Rankin SL, Ju B, Li Y*, et al.* The genomic landscape of diffuse intrinsic pontine glioma and pediatric non-brainstem high-grade glioma. Nat Genet **2014**;46(5):444-50 doi 10.1038/ng.2938.

10. Duffner PK, Horowitz ME, Krischer JP, Burger PC, Cohen ME, Sanford RA*, et al.* The treatment of malignant brain tumors in infants and very young children: an update of the Pediatric Oncology Group experience. Neuro Oncol **1999**;1(2):152-61 doi 10.1093/neuonc/1.2.152.

11. Lafay-Cousin L, Strother D. Current treatment approaches for infants with malignant central nervous system tumors. Oncologist **2009**;14(4):433-44 doi 10.1634/theoncologist.2008-0193.

12. Isaacs H, Jr. Perinatal (fetal and neonatal) astrocytoma: a review. Childs Nerv Syst **2016**;32(11):2085-96 doi 10.1007/s00381-016-3215-y.

13. Gelabert-Gonzalez M, Serramito-Garcia R, Arcos-Algaba A. Desmoplastic infantile and non-infantile ganglioglioma. Review of the literature. Neurosurg Rev **2010**;34(2):151-8 doi 10.1007/s10143-010-0303-4.

14. Dufour C, Grill J, Lellouch-Tubiana A, Puget S, Chastagner P, Frappaz D*, et al.* High-grade glioma in children under 5 years of age: a chemotherapy only approach with

the BBSFOP protocol. Eur J Cancer **2006**;42(17):2939-45 doi 10.1016/j.ejca.2006.06.021.

15. Geyer JR, Finlay JL, Boyett JM, Wisoff J, Yates A, Mao L*, et al.* Survival of infants with malignant astrocytomas. A Report from the Childrens Cancer Group. Cancer **1995**;75(4):1045-50.

16. Grundy RG, Wilne SH, Robinson KJ, Ironside JW, Cox T, Chong WK*, et al.* Primary postoperative chemotherapy without radiotherapy for treatment of brain tumours other than ependymoma in children under 3 years: results of the first UKCCSG/SIOP CNS 9204 trial. Eur J Cancer **2010**;46(1):120-33 doi 10.1016/j.ejca.2009.09.013.

17. Guerreiro Stucklin AS, Ryall S, Fukuoka K, Zapotocky M, Lassaletta A, Li C*, et al.* Alterations in ALK/ROS1/NTRK/MET drive a group of infantile hemispheric gliomas. Nat Commun **2019**;10(1):4343 doi 10.1038/s41467-019-12187-5.

18. Macy ME, Birks DK, Barton VN, Chan MH, Donson AM, Kleinschmidt-Demasters BK*, et al.* Clinical and molecular characteristics of congenital glioblastoma. Neuro Oncol **2012**;14(7):931-41 doi 10.1093/neuonc/nos125.

19. Takeshima H, Kawahara Y, Hirano H, Obara S, Niiro M, Kuratsu J. Postoperative regression of desmoplastic infantile gangliogliomas: report of two cases. Neurosurgery **2003**;53(4):979-83; discussion 83-4.

20. Haberler C, Slavc I, Czech T, Prayer D, Pirker C, Budka H*, et al.* Malignant predominantly minigemistocytic glioma in two infants: a distinctive glioma variant? Neuropathol Appl Neurobiol **2007**;33(2):169-78 doi 10.1111/j.1365-2990.2006.00823.x.

21. Gielen GH, Gessi M, Buttarelli FR, Baldi C, Hammes J, zur Muehlen A*, et al.* Genetic Analysis of Diffuse High-Grade Astrocytomas in Infancy Defines a Novel Molecular Entity. Brain Pathol **2015**;25(4):409-17 doi 10.1111/bpa.12210.

22. Anestis DM, Tsitsopoulos PP, Ble CA, Tsitouras V, Tsonidis CA. Congenital Glioblastoma Multiforme: An Unusual and Challenging Tumor. Neuropediatrics **2017**;48(6):403-12 doi 10.1055/s-0037-1601858.

23. Wang AC, Jones DTW, Abecassis IJ, Cole BL, Leary SES, Lockwood CM*, et al.* Desmoplastic Infantile Ganglioglioma/Astrocytoma (DIG/DIA) Are Distinct Entities with Frequent BRAFV600 Mutations. Mol Cancer Res **2018**;16(10):1491-8 doi 10.1158/1541-7786.MCR-17-0507.

24. Amatu A, Sartore-Bianchi A, Siena S. NTRK gene fusions as novel targets of cancer therapy across multiple tumour types. ESMO Open **2016**;1(2):e000023 doi 10.1136/esmoopen-2015-000023.

25. Jones DT, Hutter B, Jager N, Korshunov A, Kool M, Warnatz HJ*, et al.* Recurrent somatic alterations of FGFR1 and NTRK2 in pilocytic astrocytoma. Nat Genet **2013**;45(8):927-32 doi 10.1038/ng.2682.

26. Zhang J, Wu G, Miller CP, Tatevossian RG, Dalton JD, Tang B*, et al.* Whole-genome sequencing identifies genetic alterations in pediatric low-grade gliomas. Nat Genet **2013**;45(6):602-12 doi 10.1038/ng.2611.

27. Aghajan Y, Levy ML, Malicki DM, Crawford JR. Novel PPP1CB-ALK fusion protein in a high-grade glioma of infancy. BMJ Case Rep **2016**;2016 doi 10.1136/bcr-2016-217189.

28. Chmielecki J, Bailey M, He J, Elvin J, Vergilio JA, Ramkissoon S*, et al.* Genomic Profiling of a Large Set of Diverse Pediatric Cancers Identifies Known and Novel

Mutations across Tumor Spectra. Cancer Res **2017**;77(2):509-19 doi 10.1158/0008-5472.CAN-16-1106.

29. Cocce MC, Mardin BR, Bens S, Stutz AM, Lubieniecki F, Vater I*, et al.* Identification of ZCCHC8 as fusion partner of ROS1 in a case of congenital glioblastoma multiforme with a t(6;12)(q21;q24.3). Genes Chromosomes Cancer **2016**;55(9):677-87 doi 10.1002/gcc.22369.

30. Kiehna EN, Arnush MR, Tamrazi B, Cotter JA, Hawes D, Robison NJ*, et al.* Novel GOPC(FIG)-ROS1 fusion in a pediatric high-grade glioma survivor. J Neurosurg Pediatr **2017**;20(1):51-5 doi 10.3171/2017.2.PEDS16679.

31. Maruggi M, Malicki DM, Levy ML, Crawford JR. A novel KIF5B-ALK fusion in a child with an atypical central nervous system inflammatory myofibroblastic tumour. BMJ Case Rep **2018**;2018 doi 10.1136/bcr-2018-226431.

32. Nakano Y, Tomiyama A, Kohno T, Yoshida A, Yamasaki K, Ozawa T*, et al.* Identification of a novel KLC1-ROS1 fusion in a case of pediatric low-grade localized glioma. Brain Tumor Pathol **2019**;36(1):14-9 doi 10.1007/s10014-018-0330-3.

33. Ng A, Levy ML, Malicki DM, Crawford JR. Unusual high-grade and low-grade glioma in an infant with PPP1CB-ALK gene fusion. BMJ Case Rep **2019**;12(2) doi 10.1136/bcr-2018-228248.

34. Olsen TK, Panagopoulos I, Meling TR, Micci F, Gorunova L, Thorsen J*, et al.* Fusion genes with ALK as recurrent partner in ependymoma-like gliomas: a new brain tumor entity? Neuro Oncol **2015**;17(10):1365-73 doi 10.1093/neuonc/nov039.

35. Ziegler DS, Wong M, Mayoh C, Kumar A, Tsoli M, Mould E*, et al.* Brief Report: Potent clinical and radiological response to larotrectinib in TRK fusion-driven high-grade glioma. Br J Cancer **2018**;119(6):693-6 doi 10.1038/s41416-018-0251-2.

36. Sturm D, Orr BA, Toprak UH, Hovestadt V, Jones DT, Capper D*, et al.* New Brain Tumor Entities Emerge from Molecular Classification of CNS-PNETs. Cell **2016**;164(5):1060-72 doi 10.1016/j.cell.2016.01.015.

37. Koelsche C, Mynarek M, Schrimpf D, Bertero L, Serrano J, Sahm F*, et al.* Primary intracranial spindle cell sarcoma with rhabdomyosarcoma-like features share a highly distinct methylation profile and DICER1 mutations. Acta Neuropathol **2018**;136(2):327-37 doi 10.1007/s00401-018-1871-6.

38. Johannessen AL, Torp SH. The clinical value of Ki-67/MIB-1 labeling index in human astrocytomas. Pathol Oncol Res **2006**;12(3):143-7 doi PAOR.2006.12.3.0143.

39. El-Ayadi M, Ansari M, Sturm D, Gielen GH, Warmuth-Metz M, Kramm CM*, et al.* High-grade glioma in very young children: a rare and particular patient population. Oncotarget **2017**;8(38):64564-78 doi 10.18632/oncotarget.18478.

40. Capper D, Jones DTW, Sill M, Hovestadt V, Schrimpf D, Sturm D*, et al.* DNA methylation-based classification of central nervous system tumours. Nature **2018**;555(7697):469-74 doi 10.1038/nature26000.

41. van Tilburg CM, Selt F, Sahm F, Bachli H, Pfister SM, Witt O*, et al.* Response in a child with a BRAF V600E mutated desmoplastic infantile astrocytoma upon retreatment with vemurafenib. Pediatr Blood Cancer **2018**;65(3) doi 10.1002/pbc.26893.

42. Charest A, Lane K, McMahon K, Park J, Preisinger E, Conroy H*, et al.* Fusion of FIG to the receptor tyrosine kinase ROS in a glioblastoma with an interstitial

del(6)(q21q21). Genes Chromosomes Cancer **2003**;37(1):58-71 doi 10.1002/gcc.10207.

43. International Cancer Genome Consortium PedBrain Tumor P. Recurrent MET fusion genes represent a drug target in pediatric glioblastoma. Nat Med **2016**;22(11):1314-20 doi 10.1038/nm.4204.

44. Soda M, Choi YL, Enomoto M, Takada S, Yamashita Y, Ishikawa S*, et al.* Identification of the transforming EML4-ALK fusion gene in non-small-cell lung cancer. Nature **2007**;448(7153):561-6 doi 10.1038/nature05945.

45. Qaddoumi I, Orisme W, Wen J, Santiago T, Gupta K, Dalton JD*, et al.* Genetic alterations in uncommon low-grade neuroepithelial tumors: BRAF, FGFR1, and MYB mutations occur at high frequency and align with morphology. Acta Neuropathol **2016**;131(6):833-45 doi 10.1007/s00401-016-1539-z.

46. Singh D, Chan JM, Zoppoli P, Niola F, Sullivan R, Castano A*, et al.* Transforming fusions of FGFR and TACC genes in human glioblastoma. Science **2012**;337(6099):1231-5 doi 10.1126/science.1220834.

47. Davis JL, Lockwood CM, Stohr B, Boecking C, Al-Ibraheemi A, DuBois SG*, et al.* Expanding the Spectrum of Pediatric NTRK-rearranged Mesenchymal Tumors. Am J Surg Pathol **2018** doi 10.1097/PAS.0000000000001203.

48. Farago AF, Azzoli CG. Beyond ALK and ROS1: RET, NTRK, EGFR and BRAF gene rearrangements in non-small cell lung cancer. Transl Lung Cancer Res **2017**;6(5):550-9 doi 10.21037/tlcr.2017.08.02.

49. Pietrantonio F, Di Nicolantonio F, Schrock AB, Lee J, Tejpar S, Sartore-Bianchi A*, et al.* ALK, ROS1, and NTRK Rearrangements in Metastatic Colorectal Cancer. J Natl Cancer Inst **2017**;109(12) doi 10.1093/jnci/djx089.

50. Davare MA, Henderson JJ, Agarwal A, Wagner JP, Iyer SR, Shah N*, et al.* Rare but Recurrent ROS1 Fusions Resulting From Chromosome 6q22 Microdeletions are Targetable Oncogenes in Glioma. Clin Cancer Res **2018**;24(24):6471-82 doi 10.1158/1078-0432.CCR-18-1052.

51. Gatalica Z, Xiu J, Swensen J, Vranic S. Molecular characterization of cancers with NTRK gene fusions. Mod Pathol **2019**;32(1):147-53 doi 10.1038/s41379-018-0118-3.

52. Johnson A, Severson E, Gay L, Vergilio JA, Elvin J, Suh J*, et al.* Comprehensive Genomic Profiling of 282 Pediatric Low- and High-Grade Gliomas Reveals Genomic Drivers, Tumor Mutational Burden, and Hypermutation Signatures. Oncologist **2017**;22(12):1478-90 doi 10.1634/theoncologist.2017-0242.

53. Okamura R, Boichard A, Kato S, Sicklick JK, Bazhenova L, Kurzrock R. Analysis of NTRK Alterations in Pan-Cancer Adult and Pediatric Malignancies: Implications for NTRK-Targeted Therapeutics. JCO Precis Oncol **2018**;2018 doi 10.1200/PO.18.00183.

54. McArthur GA, Laherty CD, Queva C, Hurlin PJ, Loo L, James L*, et al.* The Mad protein family links transcriptional repression to cell differentiation. Cold Spring Harb Symp Quant Biol **1998**;63:423-33.

55. Gripp KW, Aldinger KA, Bennett JT, Baker L, Tusi J, Powell-Hamilton N*, et al.* A novel rasopathy caused by recurrent de novo missense mutations in PPP1CB closely resembles Noonan syndrome with loose anagen hair. Am J Med Genet A **2016**;170(9):2237-47 doi 10.1002/ajmg.a.37781.

56. Dehmelt L, Halpain S. The MAP2/Tau family of microtubule-associated proteins. Genome Biol **2005**;6(1):204 doi 10.1186/gb-2004-6-1-204.

57. Saadi I, Alkuraya FS, Gisselbrecht SS, Goessling W, Cavallesco R, Turbe-Doan A*, et al.* Deficiency of the cytoskeletal protein SPECC1L leads to oblique facial clefting. Am J Hum Genet **2011**;89(1):44-55 doi 10.1016/j.ajhg.2011.05.023.

58. Wilson NR, Olm-Shipman AJ, Acevedo DS, Palaniyandi K, Hall EG, Kosa E*, et al.* SPECC1L deficiency results in increased adherens junction stability and reduced cranial neural crest cell delamination. Sci Rep **2016**;6:17735 doi 10.1038/srep17735.

59. Kalashnikova E, Lorca RA, Kaur I, Barisone GA, Li B, Ishimaru T*, et al.* SynDIG1: an activity-regulated, AMPA- receptor-interacting transmembrane protein that regulates excitatory synapse development. Neuron **2010**;65(1):80-93 doi 10.1016/j.neuron.2009.12.021.

60. Metzler M, Li B, Gan L, Georgiou J, Gutekunst CA, Wang Y*, et al.* Disruption of the endocytic protein HIP1 results in neurological deficits and decreased AMPA receptor trafficking. EMBO J **2003**;22(13):3254-66 doi 10.1093/emboj/cdg334.

61. Nakai T, Nagai T, Tanaka M, Itoh N, Asai N, Enomoto A*, et al.* Girdin phosphorylation is crucial for synaptic plasticity and memory: a potential role in the interaction of BDNF/TrkB/Akt signaling with NMDA receptor. J Neurosci **2014**;34(45):14995-5008 doi 10.1523/JNEUROSCI.2228-14.2014.

62. Enomoto A, Murakami H, Asai N, Morone N, Watanabe T, Kawai K*, et al.* Akt/PKB regulates actin organization and cell motility via Girdin/APE. Dev Cell **2005**;9(3):389-402 doi 10.1016/j.devcel.2005.08.001.

63. Ren X, Kuan PF. methylGSA: a Bioconductor package and Shiny app for DNA methylation data length bias adjustment in gene set testing. Bioinformatics **2019**;35(11):1958-9 doi 10.1093/bioinformatics/bty892.

64. Mackay A, Burford A, Molinari V, Jones DTW, Izquierdo E, Brouwer-Visser J*, et al.* Molecular, Pathological, Radiological, and Immune Profiling of Non-brainstem Pediatric High-Grade Glioma from the HERBY Phase II Randomized Trial. Cancer Cell **2018**;33(5):829-42 e5 doi 10.1016/j.ccell.2018.04.004.

65. Louis DN, Perry A, Reifenberger G, von Deimling A, Figarella-Branger D, Cavenee WK*, et al.* The 2016 World Health Organization Classification of Tumors of the Central Nervous System: a summary. Acta Neuropathol **2016**;131(6):803-20 doi 10.1007/s00401-016-1545-1.

66. Infarinato NR, Park JH, Krytska K, Ryles HT, Sano R, Szigety KM*, et al.* The ALK/ROS1 Inhibitor PF-06463922 Overcomes Primary Resistance to Crizotinib in ALK-Driven Neuroblastoma. Cancer Discov **2016**;6(1):96-107 doi 10.1158/2159-8290.CD-15-1056.

67. Kilkenny C, Browne WJ, Cuthill IC, Emerson M, Altman DG. Improving bioscience research reporting: the ARRIVE guidelines for reporting animal research. PLoS Biol **2010**;8(6):e1000412 doi 10.1371/journal.pbio.1000412.

68. Workman P, Aboagye EO, Balkwill F, Balmain A, Bruder G, Chaplin DJ*, et al.* Guidelines for the welfare and use of animals in cancer research. Br J Cancer **2010**;102(11):1555-77 doi 10.1038/sj.bjc.6605642.

Legends for Figures

Figure 1 – Defining an intrinsic set of infant gliomas. (A) Flow diagram providing an overview of the inclusion and exclusion criteria for the assembled cohort of 241 samples from patients under the age of 4 years. (B) Fusion gene analysis by a variety of means allowed for the identification of 28 fusions marking clearly defined entities that were subsequently excluded from further analysis. (C) Methylation array profiling and analysis by the Heidelberg classifier excluded a further 12 cases closely resembling non-glioma entities or failing quality control (n=9). (D) t-statistic based stochastic neighbor embedding (tSNE) projection of the remaining cases highlighted 61 samples which clustered with previously reported high or low grade glioma subtypes, leaving an intrinsic set of 130 infant gliomas for further characterisation by more histopathological assessment and in-depth sequencing. (E) Anatomical location of infant gliomas after exclusion of pathognomonic fusions and non-glioma entities by methylation profiling (n=130). Left – sagittal section showing internal structures; right – external view highlighting cerebral lobes. Each circle represents a single case and is colored by the glioma subgroup it most closely clusters with, defined by the key below. (F) Kaplan-Meier plot of overall survival of cases separated by methylation subgroups DIGG (desmoplastic infantile ganglioglioma / astrocytoma), IHG (infant hemispheric glioma), LGG (other low grade glioma subgroups) and HGG (other high grade glioma subgroups) (n=102). P value is calculated by the log-rank test (p=0.0566 for HGG *versus* rest). (G) t-statistic based stochastic neighbor embedding (t-SNE) projection of a combined methylation dataset comprising the intrinsic set of the present study (n=130, circled) plus a reference set of glioma subtypes (n=1652). The first two projections are plotted on the x and y axes, with samples represented by dots colored by subtype according to the key provided.

Figure 2 – Mutations in infant gliomas. (A) Oncoprint representation of an integrated annotation of single nucleotide variants, DNA copy number changes and structural variants for infant gliomas excluded as other subgroups (n=24). (B) Oncoprint representation of an integrated annotation of single nucleotide variants, DNA copy number changes and structural variants for infant gliomas in the intrinsic set (n=41). Samples are arranged in columns with genes labelled along rows. Clinicopathological and molecular annotations are provided as bars according to the included key.

Figure 3 - Copy number-associated fusion genes in infant gliomas. (A) Segmented DNA copy number heatmap for *ALK* breakpoint cases, plotted according to chromosomal location. Pink, gain; blue, loss. (B) Segmented DNA copy number heatmap for *ROS1* breakpoint cases, plotted according to chromosomal location. Pink, gain; blue, loss. (C) Segmented DNA copy number heatmap for *MET* breakpoint cases, plotted according to chromosomal location. Pink, gain; blue, loss. (D) *ETV6:NTRK3*. Cartoon representation of the fusion structure, with reads on either side of the breakpoint colored by gene partner and taken from an Integrated Genome Viewer (IGV) snapshot. Below this is a Sanger sequencing trace spanning the breakpoint. Underneath are copy number plots (log2 ratio, y axis) for chromosomal regions spanning the breakpoints (x axis). Points are colored red for copy number gain, blue for loss, and grey for no change. The smoothed values are overlaid by the purple line. (E) *ZC3H7A:ALK*. Cartoon representation of the fusion structure, with reads on either side of the breakpoint colored by gene partner and taken from an Integrated Genome Viewer snapshot. Below this is a Sanger sequencing trace spanning the breakpoint. Underneath are copy number plots (log2 ratio, y axis) for chromosomal regions spanning the breakpoints (x axis). Points are colored red for copy number gain, blue for loss, and grey for no change. The smoothed values are overlaid by the purple line. (F) Circos plot of gene fusions targeting *NTRK1* (light

orange), *NTRK2* (orange) and *NTRK3* (dark orange). Lines link fusion gene partners according to chromosomal location, represented by ideograms arranged around the circle. (G) Circos plot of gene fusions targeting *ALK* (dark blue). Lines link fusion gene partners according to chromosomal location, represented by ideograms arranged around the circle. (H) Kaplan-Meier plot of overall survival of cases separated by fusion event (n=63). P value is calculated by the log-rank test (p=0.085 for any fusion *versus* None).

Figure 4 – Epigenetic alterations in fusion-positive and -negative infant gliomas. (A) Differential methylation-based gene ontology analysis for *ALK*-fusion cases, represented in barplots of -log10 p value for labelled highest scoring categories (top) and aggregated ontology networks (bottom). (B) Differential methylation-based gene ontology analysis for *NTRK*-fusion cases, represented in barplots of -log10 p value for labelled highest scoring categories (top) and aggregated ontology networks (bottom). (C) Differential methylation-based gene ontology analysis for fusion-negative cases, represented in barplots of -log10 p value for labelled highest scoring categories (top) and aggregated ontology networks (bottom). Node size is proportional to the number of genes, shading represents -log10 p value (darker is higher). Thickness of connecting lines reflects the percentage of overlapping genes. (D) Genome browser view of the *WNT5A* locus, with lower methylation, provided as barplots, in selected *ALK*-fusion (blue) cases compared to *NTRK*-fusion (orange) and fusion-negative (grey) cases. (E) Genome browser view of the *STAT1* locus, with lower methylation, provided as barplots, in selected *NTRK*-fusion (orange) cases compared to *ALK*-fusion (blue) and fusion-negative (grey) cases. (F) Genome browser view of the *TP63* locus, with lower methylation, provided as barplots, in selected fusion-negative (grey) cases compared to *ALK*-fusion (blue) and *NTRK*-fusion (orange) cases. Chromosomal ideograms are provided with the red bar indicating the cytoband in which the locus is found. Differentially methylated probes

are highlighted by the red box. (G) Immunofluorescent staining of an antibody directed against WNT5A (white) in an *EML4:ALK* fusion infant glioma case, UOLP_INF_001. DAPI is used as a counterstain. Scale bar = 200µM. (H) Immunofluorescent staining of an antibody directed against WNT5A (green) in an *ETV6:NTRK3* fusion infant glioma case, GOSH_INF_007. DAPI is used as a counterstain. Scale bar = 200µM. (I) Heatmap representing gene expression values from a NanoString assay of 30 most differentially methylated genes between *ALK*-fusion (blue), *NTRK*-fusion (orange) and fusion-negative (grey) cases. Expression values are colored according to the scale provided.

Figure 5 - Pre-clinical modelling of *ALK*-fused glioma. (A) Schematic representation of the *in vivo* modelling workflow. IUE, *in utero* electroporation; KD, kinase domain. (B) Kaplan-Meier curve of injected animals using IUE and p0-RCAS method – *PPP1CB:ALK* only IUE, *PPP1CB:ALK* + *Trp53*-ko IUE, *PPP1CB:ALK* + *Cdkn2a*-ko IUE and *PPP1CB:ALK* p0-RCAS only. *, $p<0.05$, **, $p<0.01$ (C, D) Effect of targeted ALK inhibition on growth of allografted *PPP1CB:ALK* + *Cdkn2a*-ko mouse tumor cells *in vivo*. p.i., post injection. (E) Targeted inhibition significantly prolonged the survival of *PPP1CB:ALK* + *Cdkn2a*-ko allografted mice compared with temozolomide or vehicle controls. Two mice in the lorlatinib group were sacrificed due to technical complications with drug delivery, with no tumor being evident upon dissection of the brain. ***, $p<0.001$. (F) Clinical history of DKFZ_INF_307, with confirmed *MAD1L1:ALK* fusion. Timeline of clinical interventions is provided below, with treatment shaded in grey. Axial T2 MRI scans from diagnosis and successive surgeries and chemotherapeutic regimens are provided, in addition to treatment with the ALK inhibitor ceritinib, with tumor circled in red.

Figure 6 – Preclinical and clinical experience with Trk inhibitors in fusion-positive infant glioma. (A) Light microscopy image of two patient-derived infant glioma cell cultures, harboring either *TPM3:NTRK1* (QCTB-R102, light orange) or *ETV6:NTRK3* (QCTB-R077, dark red) fusions. (B) Concentration-response curves for three Trk inhibitors tested against two *NTRK* fusion-positive infant glioma cell cultures (QCTB-R102, *TPM3:NTRK1,* light orange; QCTB-R077, *ETV6:NTRK3*, dark red) and two fusion-negative glioma cultures (QCTB-R006, light grey; QCTB-R059, dark grey). Concentration of compound is plotted on a log scale (x axis) against cell viability (y axis). Mean plus standard error are plotted from at least n=3 experiments. (C) Clinical history of OPBG_INF_035, with confirmed *ETV6-NTRK3* fusion. Timeline of clinical interventions is provided below, with Trk inhibitor treatment shaded in grey. Diagnosis, post-biopsy, pre/post-surgery, post-crizotinib and post-larotrectinib axial T2 MRI scans are provided, with tumor circled in red. (D) Clinical history of MSKC_INF_006, with confirmed *ETV6:NTRK3* fusion. Timeline of clinical interventions is provided below, with Trk inhibitor treatment shaded in grey. Diagnosis and post-larotrectinib post-contrast axial T1 MRI scans are provided, with tumor circled in red.

Figure 7 – Summary of infant HGG subgroups.

Figure 1

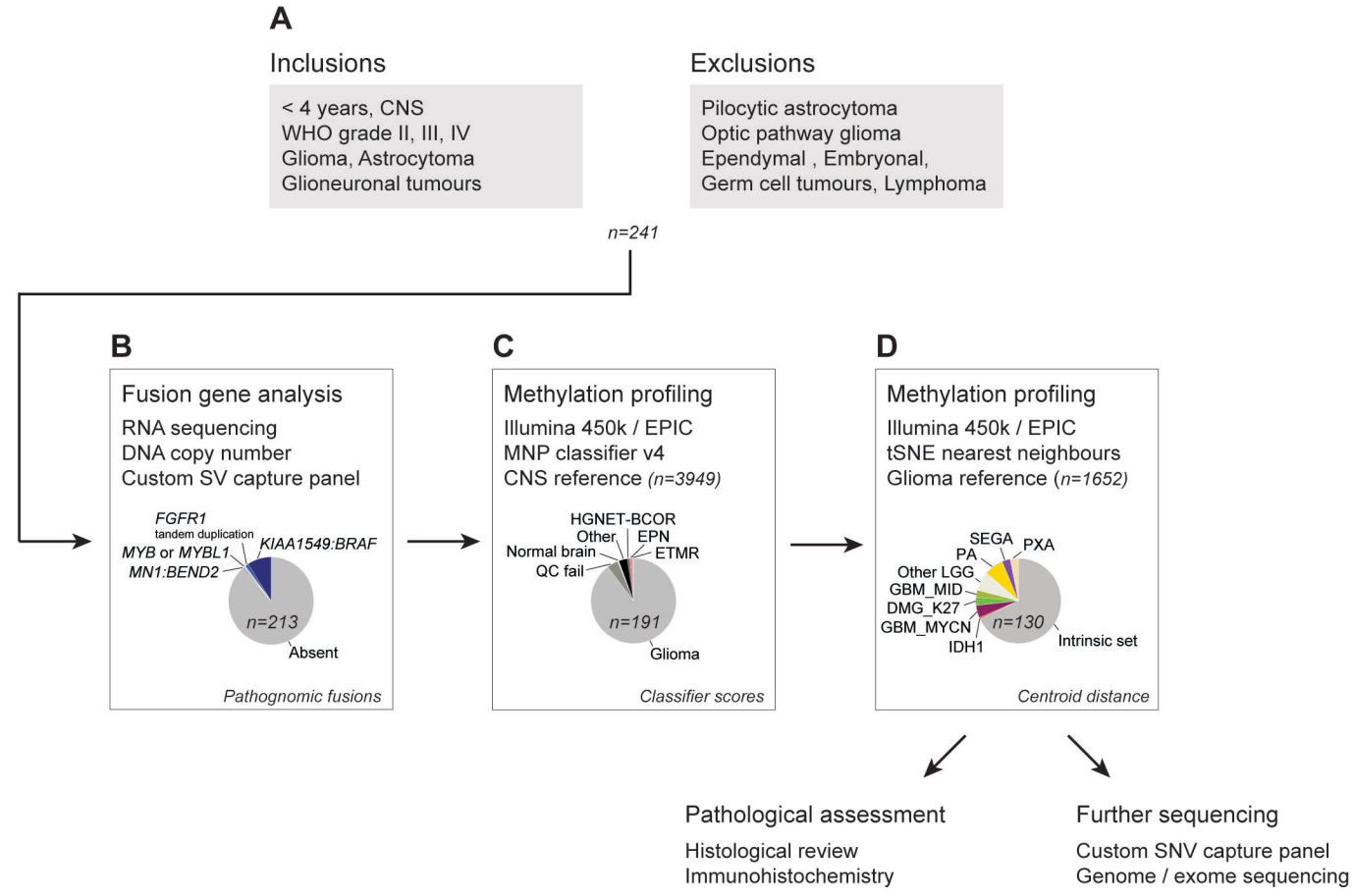

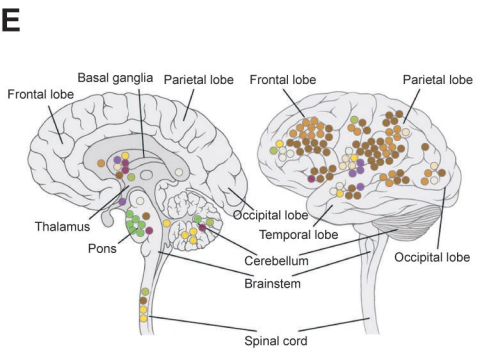

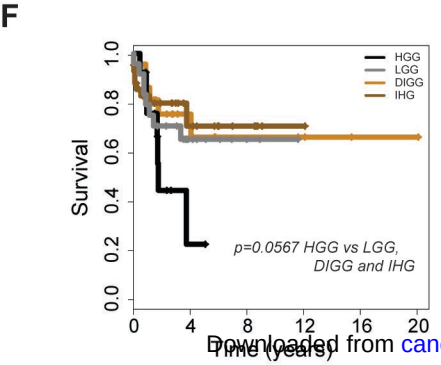

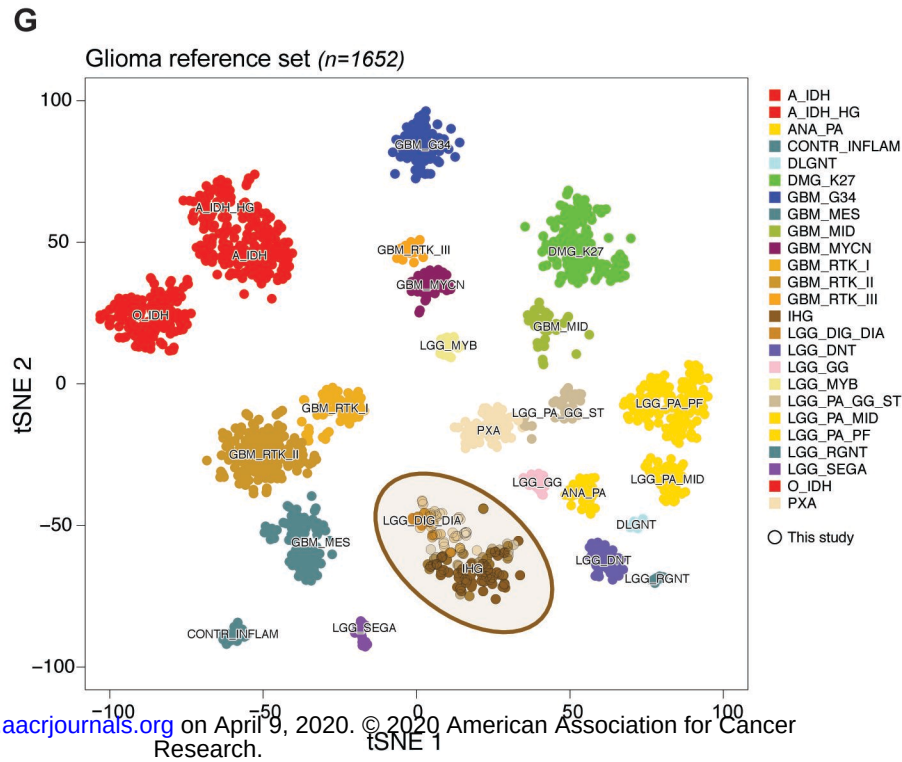

Figure 2

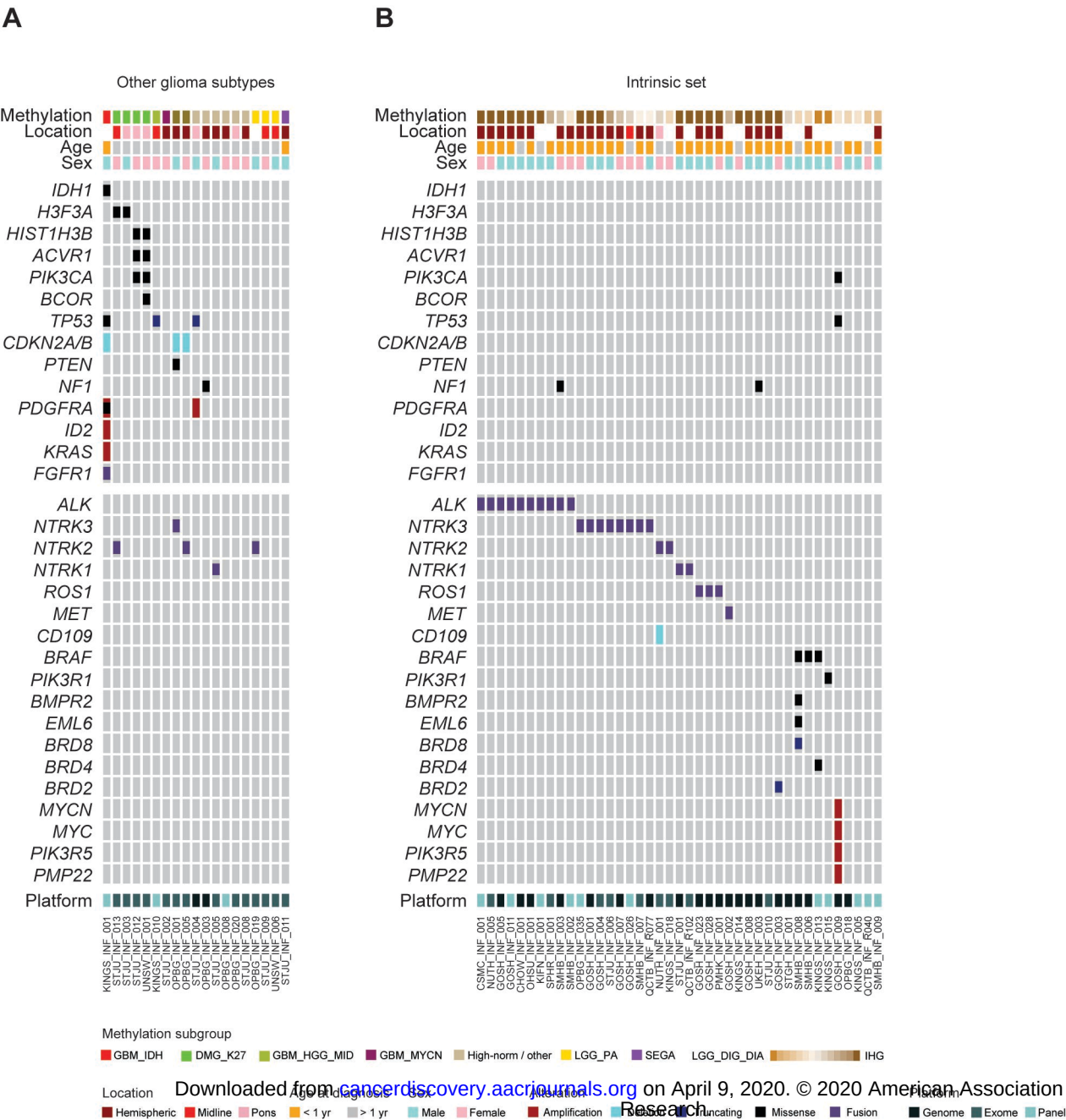

Figure 3

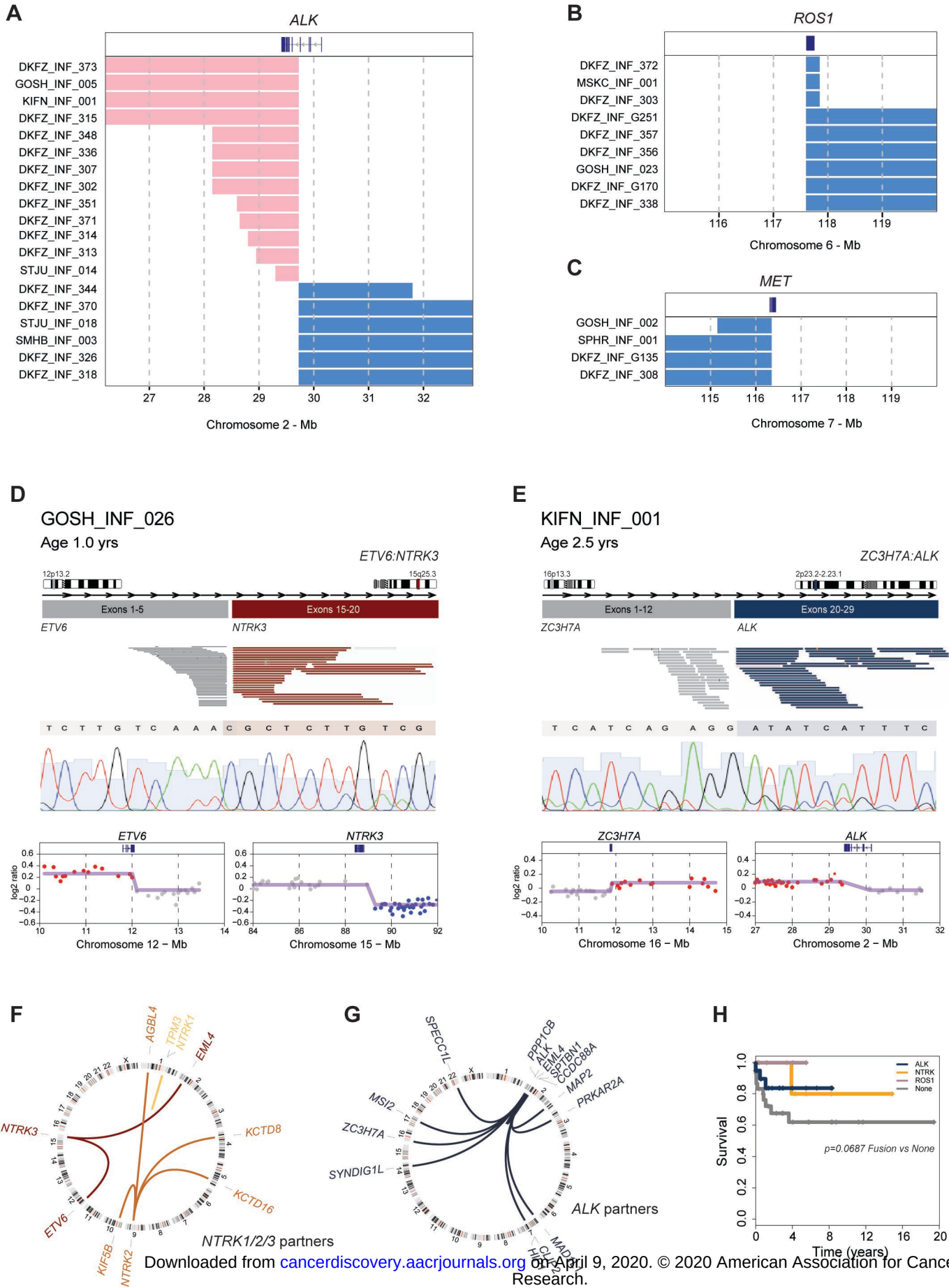

Figure 4

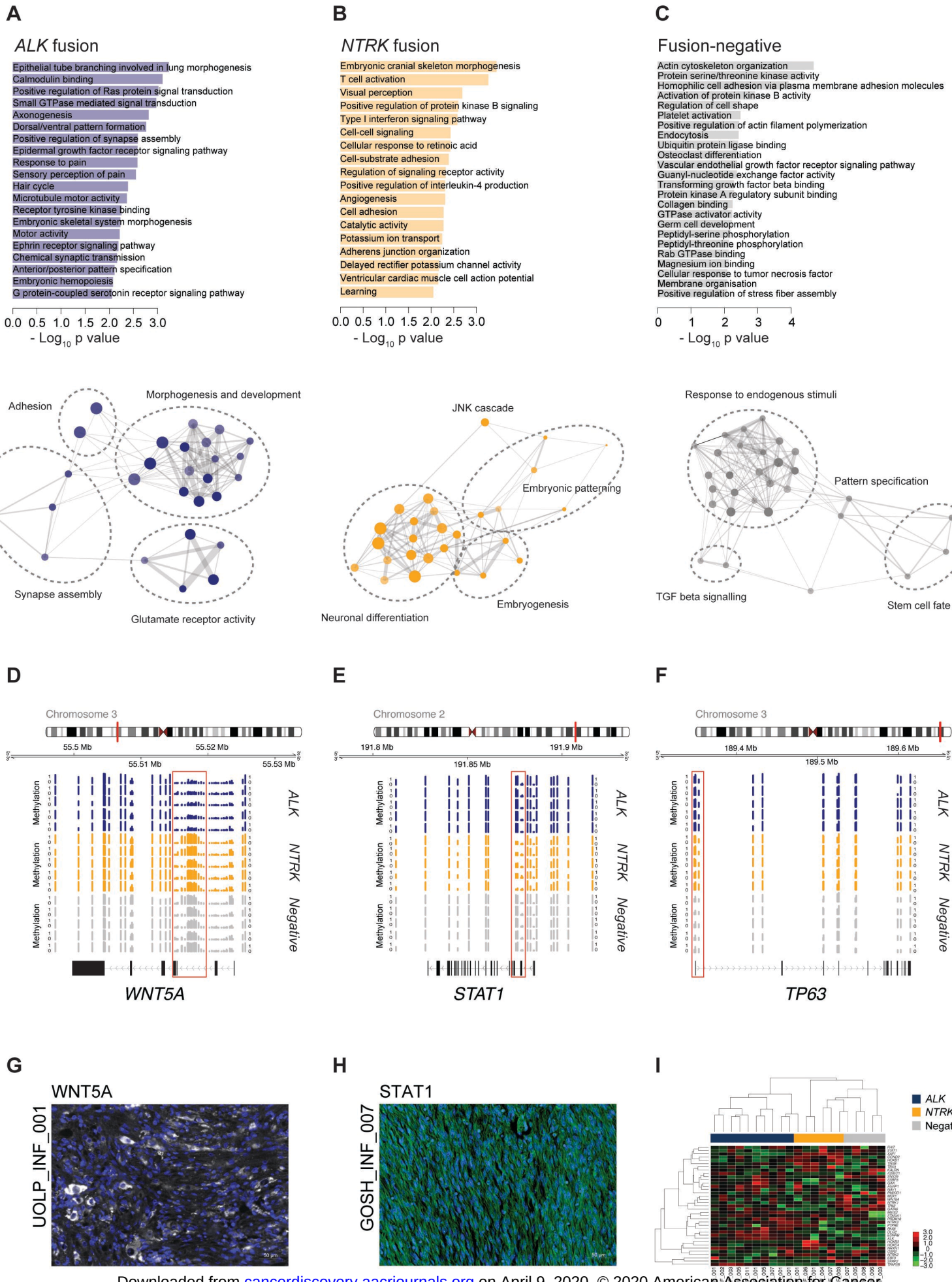

Figure 5

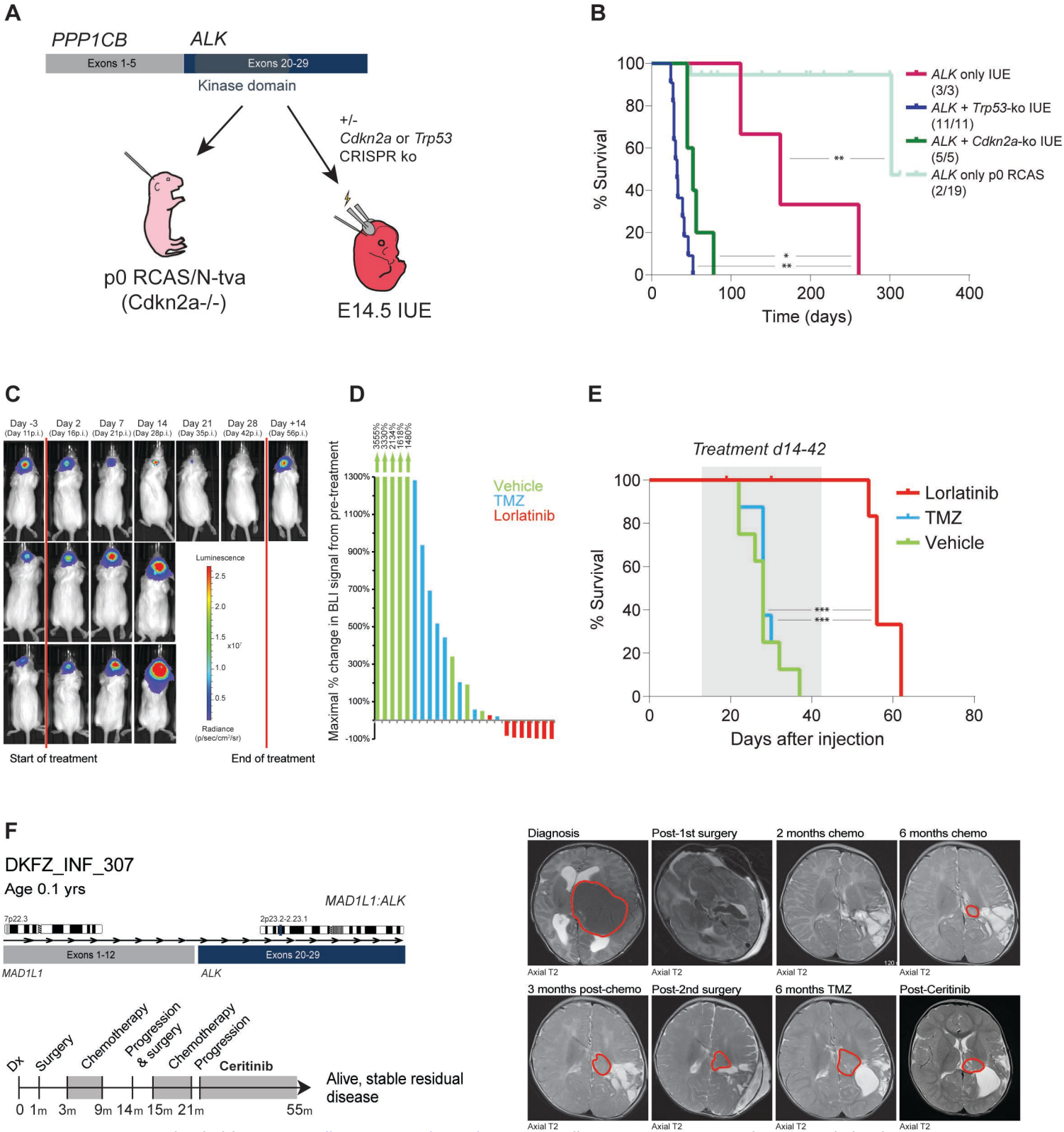

Figure 6

A

QCTB-R102
(TPM3:NTRK1)

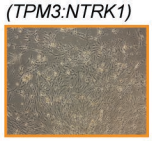

QCTB-R077
(ETV6:NTRK3)

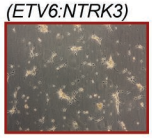

B

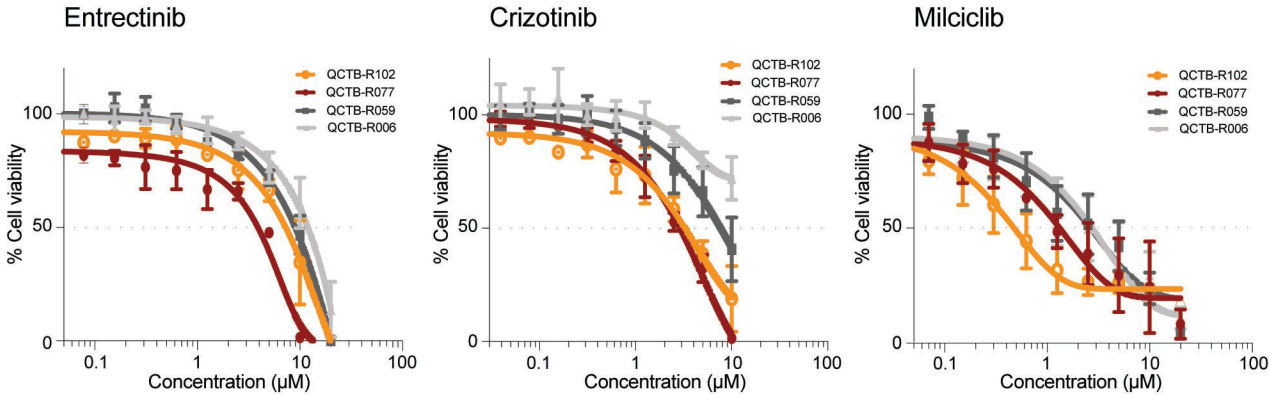

C

OPBG_INF_035
Age 0.5 yrs

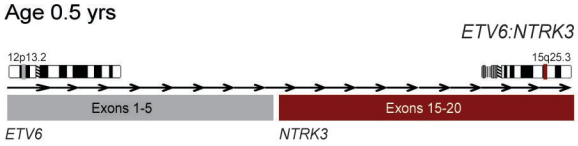

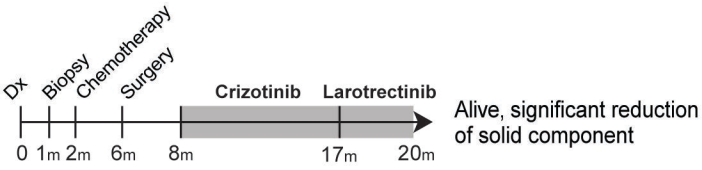

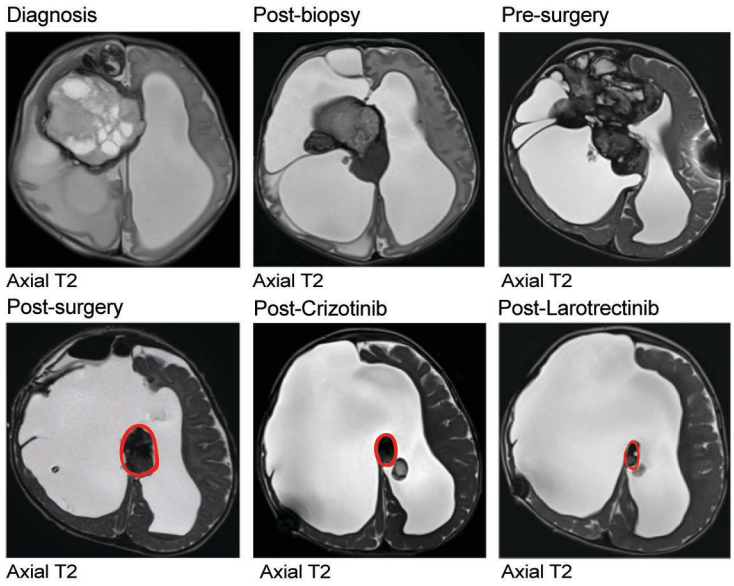

D

MSKC_INF_006
Age 0.9 yrs

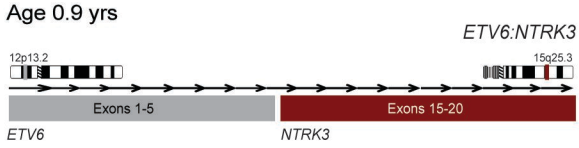

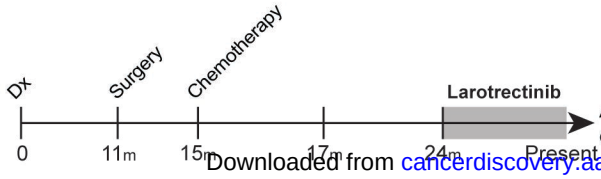

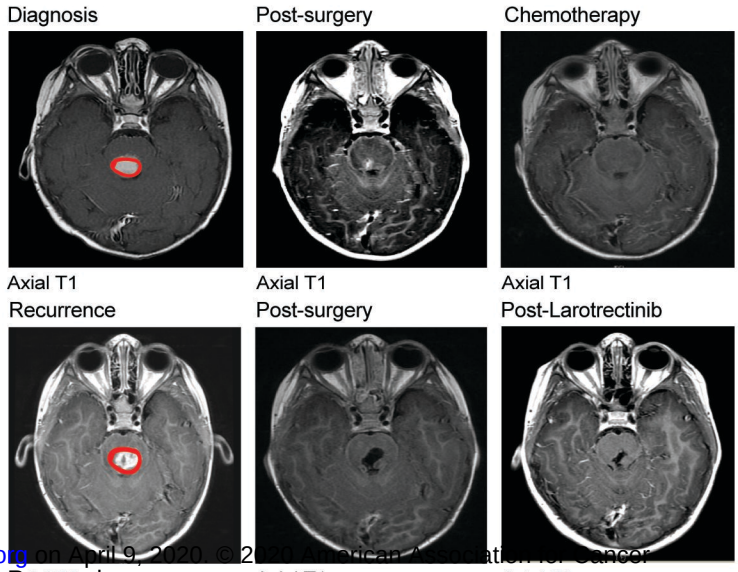

Figure 7

High grade glioma in the infant population

All locations
> 1 year

Hemispheric
< 1 year

Other glioma subgroups	*DIGG/DIA & DIGG/DIA-like*	*Intrinsic set Fusion positive*		*Intrinsic set Fusion negative*
Subgroup-specific additional mutations	*BRAF* V600E Low mutational burden	Few mutations	Few mutations	Few mutations
			ALK	
			ROS1	
		MET		
		NTRK1		
NTRK2				
		NTRK3		
FGFR1				
		Differential methylation *STAT1*, JNK	Differential methylation *WNT5A*, GluRs	Differential methylation *TP63*, TGF beta
		Neurogenesis	Synaptic plasticity	Stem cell pluripotency
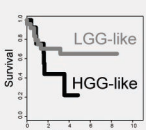		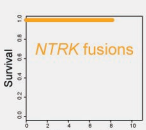	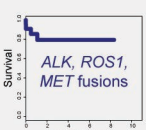	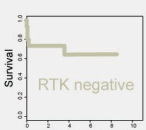
		Spindle/gemistrocytic Limited infiltrative	Spindle/gemistrocytic Limited infiltrative	Spindle/gemistocytic

AACR American Association for Cancer Research

CANCER DISCOVERY

Infant high grade gliomas comprise multiple subgroups characterized by novel targetable gene fusions and favorable outcomes

Matthew Clarke, Alan Mackay, Britta Ismer, et al.

Cancer Discov Published OnlineFirst April 1, 2020.